Synthesis and Characterization of Cyclopentadienyl Dicarbonyldiphenylphosphinopropyliron for Migratory Insertion Polymerization

by

Yibo Liu

A thesis

presented to the University of Waterloo

in fulfillment of the

thesis requirement for the degree of

Master of Science

in

Chemistry

Waterloo, Ontario, Canada, 2013

Author's Declaration

I hereby declare that I am the sole author of this thesis. This is a true copy of the thesis, including any required final revisions, as accepted by my examiners.

I understand that my thesis may be made electronically available to the public.

Abstract

Metal-containing polymers (MCPs) are emerging as a class of interesting materials with promising properties and functions. Although many techniques are available for their synthesis, the range of main-chain MCPs available for material applications is limited. Most well-defined main-chain MCP syntheses rely only on the ring-opening polymerization (ROP) of metallocene monomers, thereby new synthetic approaches for novel MCPs are in high demand. In this study a new polymerization technique, migratory insertion polymerization (MIP), was explored and used to produce novel types of MCPs with asymmetric iron repeat-units connected by phosphine-iron (Ph_2P-Fe) and iron-acyl (Fe-CO) bonds in the backbone. This research work involved the synthesis, characterization and polymerization of cyclopentadienyl(dicarbonyl)(diphenylphosphinopropyl)iron (FpP). FpP consists of an Fp functional group capable of undergoing a migratory insertion reaction (MIR) and a phosphine group to assist the MIR. FpP was prepared via the reaction between cyclopentadienyl dicarbonyl iron metalate (Fp anion) and (3-chloropropyl)diphenylphosphine, and was characterized using Fourier transform infrared (FTIR), ^{1}H NMR, ^{31}P NMR, ^{13}C NMR, and ultraviolet-visible (UV-Vis) spectroscopies. The molecules undergo intramolecular cyclization reactions at low concentrations in organic solvents, while polymerization occurs in bulk at 70 ℃, leading to polymers with number-average molecular weights (M_n) up to 12,000 g/mol and narrow molecular weight distributions (PDI=1.08-1.33). These polymers are soluble in a wide range of organic solvents and have a T_g of 100 ℃.

Acknowledgements

I would like to express my sincerest gratitude to my supervisor Prof. Xiaosong Wang for his guidance and discussion. I would like to extend my sincerest gratitude to the members of my supervisory committee, Prof. Mario Gauthier and Prof. William P. Power, for their guidance and support during my studies. I would also like to express my gratitude to Prof. Graham Murphy, Prof. Mario Gauthier, Prof. Eric Fillion, Prof. Sonny Lee, Prof. Mike Chong, Prof. Juewen Liu and their research groups; this research project would not have been possible without their support. I would also like to express my special gratitude to Prof. Frederick McCourt for his suggestions on my thesis writing and editing. I would also like to thank Janet Venne, Dr. Jalil Assoud and Dr. Richard W. Smith for their kind and patient technical support.

I would like to thank Lay Ling Tan, Nigel Singh, and Brian Tsang for their suggestions on my thesis. Special thanks also go to all my lab mates: Brian Tsang, Kai Cao, Nigel Singh, Daniel Chelladurai, Brahamjot Nayyar, Nicholas Lanigan and Sean Liew. I also wish to thank all my friends who helped me get through every day with their understanding and help. I would also like to thank Catherine Van Esch and Marguerite Greavette for ensuring that my program progressed smoothly.

Last but most importantly, I would like to express my greatest gratitude to my parents for their great help and support. They taught me an optimistic and positive attitude to life, which is infinitely precious to me.

Table of Contents

List of Figures

List of Schemes

List of Tables

List of Abbreviations

18-e	18-Electron
$AECoPF_6$	2-Acryloyloxyethyl cobaltoceniumcarboxylate hexafluorophosphate
ATRP	Atom transfer radical polymerization
CpCoCb	Cyclopentadienyl-cobalt-cyclobutadiene
Cyclic FpP5	Cyclopentadienyl(carbonyl)[3-(diphenylphosphanyl-κP)prop-1-yl]iron
Cyclic FpP6	Cyclopentadienyl(carbonyl)[(4-diphenylphosphanyl-κP)butanoyl]iron
DCM	Dichloromethane
EO	Ethylene oxide
FcGE	Ferrocenyl glycidyl ether
Fp_2	Cyclopentadienyl dicarbonyl iron dimer
FpP	Cyclopentadienyl(dicarbonyl)(diphenylphosphinopropyl)iron
FTIR	Fourier transform infrared
HMQC	Heteronuclear multiple quantum coherence
LCST	Lower critical solution temperature
MCP	Metal-containing polymer
MIP	Migratory insertion polymerization
MIR	Migratory insertion reaction
M_n	Number-average molecular weight
M_w	Weight-average molecular weight

NMR	Nuclear magnetic resonance
PDI	Polydispersity index
PEO	Poly(ethylene oxide)
PFpP	Poly(cyclopentadienylcarbonyldiphenylphosphinobutanoyliron)
PFS	Poly(ferrocenylsilane)
PVFc	Poly(vinylferrocene)
RAFT	Reversible addition-fragmentation chain transfer
ROMP	Ring-opening metathesis polymerization
ROP	Ring-opening polymerization
TEMPO	2,2,6,6-Tetramethyl-1-piperidinyloxy
T_g	Glass transition temperature
THF	Tetrahydrofuran
UV-Vis	Ultraviolet–visible
VFc	Vinylferrocene
XRD	X-ray diffraction

List of Synthesized Structures

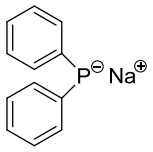

$NaPPh_2$

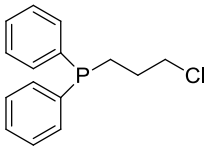

$Ph_2PCH_2CH_2CH_2Cl$

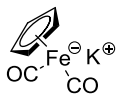

FpK

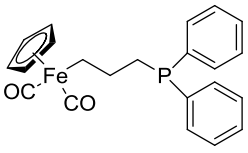

FpP

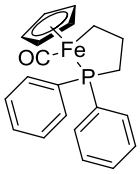

Cyclic FpP5

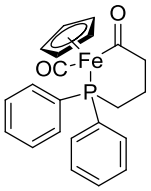

Cyclic FpP6

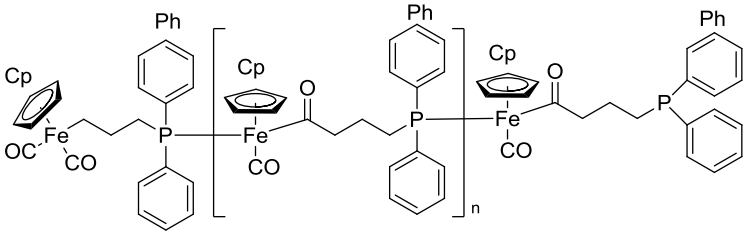

PFpP

Chapter 1. Introduction

Metal-containing polymers (MCPs) have attracted immense attention because of their interesting properties and possible applications in materials science. These hybrid materials effectively integrate physical and chemical properties of organic polymers with unique chemical, electronic, magnetic, optical, and redox properties of organometallic complexes.[1-3] Initial investigations into MCPs began in the 1950s, with the synthesis of polyvinylferrocene.[4] Since then, significant progress in the synthetic chemistry of MCPs has been accomplished. In particular, many effective synthetic approaches for MCPs have been developed since the mid-1990s.[3,5-7] Examples of such progress include condensation polymerizations,[8,9] ring-opening polymerizations (ROP),[10,11] living anionic polymerizations[12], and controlled radical polymerizations.[13-15] In addition, the parallel development of new characterization techniques has contributed to the progress in the area of MCPs.[16,17] Such developments in synthetic chemistry and unique properties of these hybrid materials have led to MCPs being used in modern technologies, including magnetic devices,[18] self-healing materials[19] and security ink.[20]

1.1 Definition and classification of MCPs

MCPs contain both organic and metallic moieties in their repeating units. MCPs can be divided into two subclasses according to the location of metal atoms in the polymers. They are side-chain and main-chain MCPs.[2,6]

1.2 Side-chain MCPs

Metal elements are incorporated into polymer side chains by two main methods.[1,6] The first strategy involves direct polymerization of metal-containing monomers, giving side-chain MCPs with a dense arrangement of metal units. However, many metal-containing complexes are not compatible with available polymerization techniques, which limits the construction of side-chain MCPs via direct polymerization of metal-containing complexes. The second strategy involves post-polymerization treatment of organic polymers with metal-containing complexes. This method is efficient and widely used to prepare side-chain MCPs.[1,6]

1.2.1 Side-chain MCPs prepared by direct polymerization of metal-containing monomers

1.2.1.1 Iron-containing side-chain MCPs

Poly(vinylferrocene) (PVFc) was the first reported high molecular weight side-chain MCP to be structure-defined. It was produced by free radical polymerization of vinylferrocene (VFc) (**Scheme 1.1**).[4] Subsequently, various strategies were developed for the synthesis of PVFc and PVFc-containing copolymers. For example, anionic polymerization and TEMPO-mediated free radical polymerization were developed to achieve the controlled polymerization of VFc.[21,22] Due to the living nature of these polymerization techniques, an extensive number of PVFc-containing block copolymers have been developed, including PVFc-poly(methyl methacrylate) (PVFc-PMMA), PVFc-polystyrene (PVFc-PS), and PVFc-polyisobutylene (PVFc-PIB) (**Scheme 1.1**).[21,23] Most recently, novel amphiphilic

PVFc-containing block and miktoarm star polymers have been reported by Frey and coworkers.[24] Their synthesis involves end-functionalization of "living" PVFc anions with one or two hydroxyl groups, followed by anionic ROP of ethylene oxide (EO) initiated by terminal hydroxyl groups to afford PVFc-poly(ethylene oxide) (PVFc-PEO) block copolymers or PVFc-$(PEO)_2$ miktoarm star polymers (**Scheme 1.2**).[24] Until now, side-chain Fc-containing polymers were derived mainly from the polymerization of VFc, though some polymerizations of ferrocenylmethyl methacrylates were also reported.[25,26] Very recently, the first Fc-containing epoxide monomer ferrocenyl glycidyl ether (FcGE) was reported.[27] This FcGE monomer can be polymerized to afford homopolymers or copolymerized with EO to yield side-chain Fc-containing random copolymers (**Scheme 1.3**). These types of copolymer with low ferrocenyl monomer contents (< 10 mol %) are soluble in water, and exhibit thermoresponsive behavior with tunable lower critical solution temperatures (LCSTs).[27] In addition, copolymers with an even lower ferrocenyl monomer content (< 5 mol %) show good biocompatibility, thus providing the opportunity for biomedical applications.[27]

Scheme 1.1 Synthesis of PVFc and PVFc-containing block copolymers.

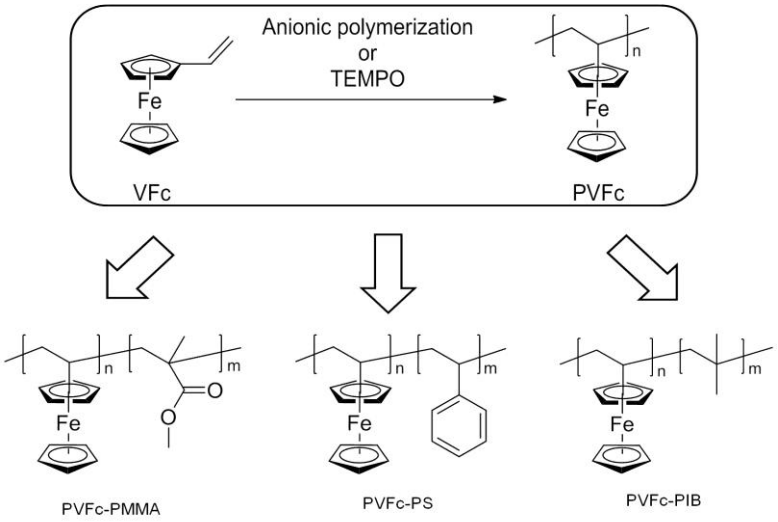

Scheme 1.2 Synthesis of amphiphilic PVFc-PEO block copolymers and PVFc-$(PEO)_2$ miktoarm star polymers.[24]

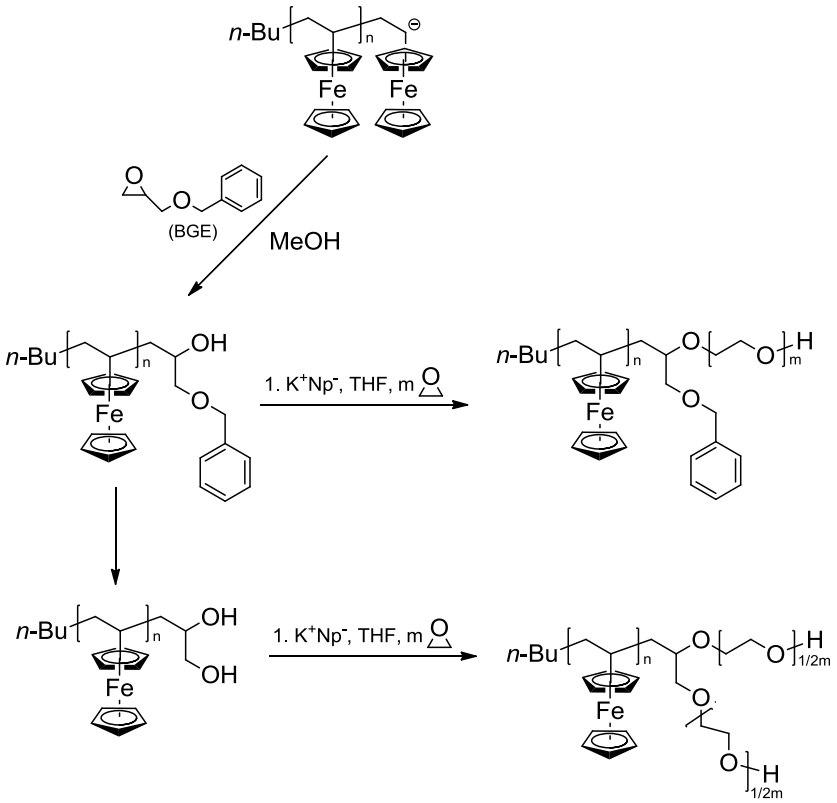

Scheme 1.3 Synthesis of PFcGE and P(EO-*co*-FcGE) homo- and copolymers by anionic ROP.[27]

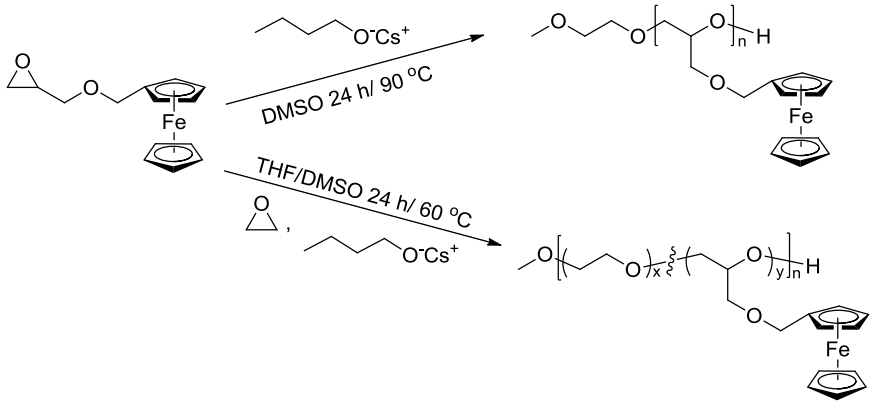

1.2.1.2 Cobalt-containing side-chain MCPs

In contrast to side-chain Fc-containing polymers, other metallocene-containing polymers have not been as extensively investigated. Recently, Tang and coworkers made considerable contributions to the synthesis of side-chain cobaltocenium-containing polymers.[28-31] Unlike 18-electron (18-e) Fc, cobaltocene is a 19-e metallocene, which can readily be oxidized into 18-e cobaltocenium. The resulting class of polyelectrolytes has unique counterion-dependent solubility, and is highly stable against further oxidation. In 2010, Tang and coworkers reported the first free radical polymerization of the cobaltocenium acrylate monomer, 2-acryloyloxyethyl cobaltoceniumcarboxylate hexafluorophosphate ($AECoPF_6$), to afford side-chain cobaltocenium-containing polymers.[29] Although the solubility of these polymers can be manipulated by an ion-exchange process, the polymerization process is not controlled and produces only low molecular weight polymers.[29] To overcome this problem, living ring-opening metathesis polymerization (ROMP) of norbornene monomers containing cobaltocenium has been developed, producing well-defined and high molecular

weight side-chain cobaltocenium-containing homo- and block- polymers (**Scheme 1.4**).[28] In addition, controlled/living radical polymerization using reversible addition-fragmentation chain transfer (RAFT) has been employed recently to prepare cobaltocenium-containing polymers (**Scheme 1.5**).[31] This strategy also resulted in novel cobaltocenium- and Fc-containing heterobimetallic diblock copolymers. Cobaltocenium-containing block copolymer micelles can be used as precursors to prepare cobalt(II or III)-containing inorganic nanoparticles using UV/ozonolysis or thermal pyrolysis.[30]

Scheme 1.4 Synthesis of cobaltocenium-containing block copolymers via ROMP involving cobaltocenium-containing norbornene monomers.[28]

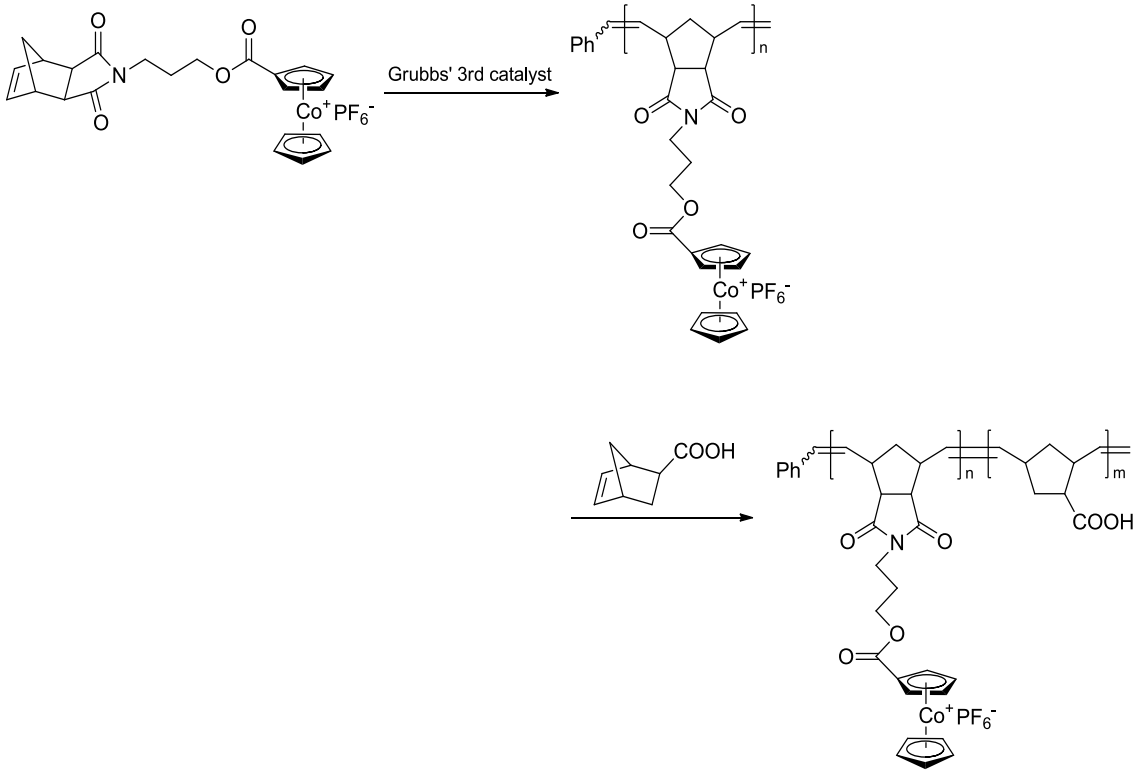

Scheme 1.5 Synthesis of side-chain cobaltocenium-containing homopolymers and diblock copolymers by RAFT polymerization.[31]

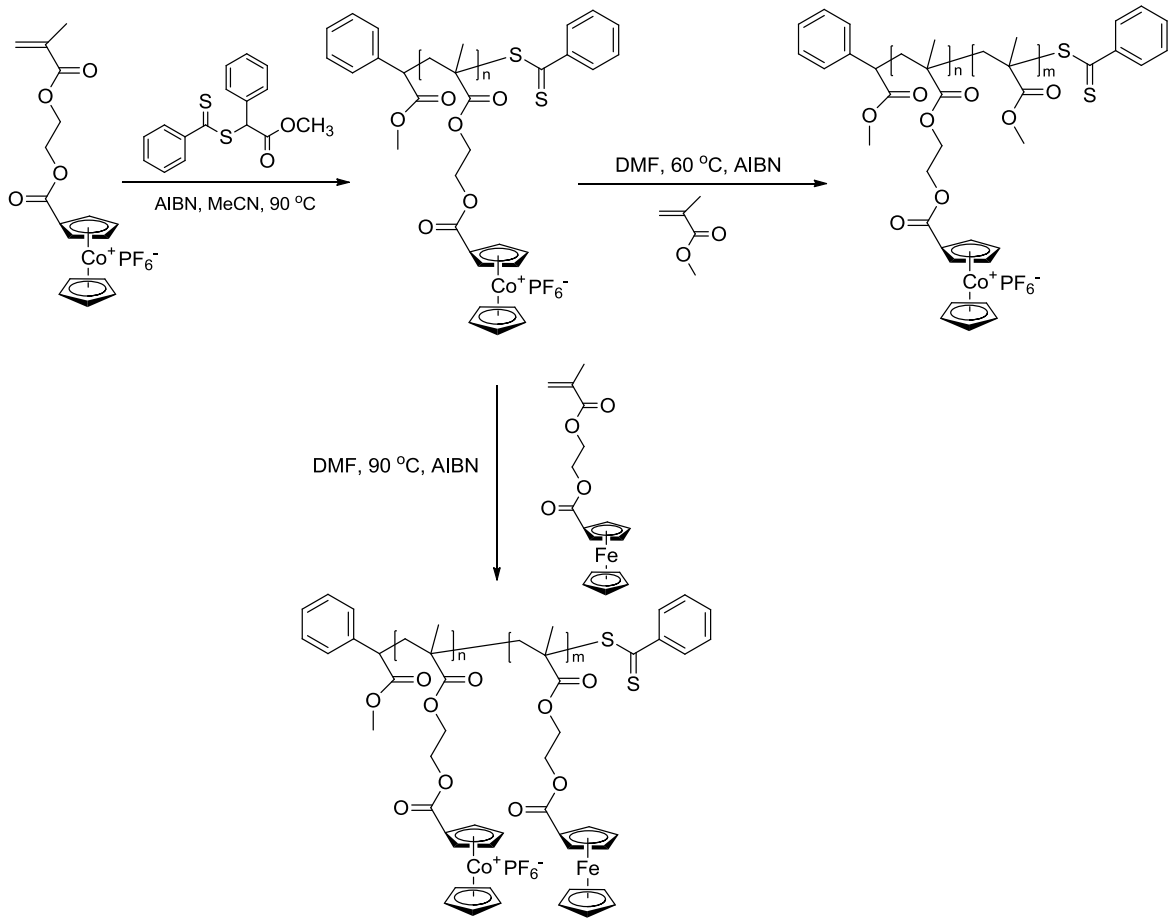

Other side-chain Co-containing polymers have been reported, including cyclopentadienyl-cobalt-cyclobutadiene (CpCoCb)-containing polymers prepared by free radical polymerization and atom transfer radical polymerization (ATRP) (**Figure 1.1A**).[32] The properties of CpCoCb give it enhanced functionality as compared to the cobaltocenium group, for example, a variety of substituents can be incorporated on the Cb ring. This property may be useful for polymer structure modification. Tew and coworkers synthesized side-chain metal-containing block copolymers composed of well-defined

alkyl-functionalized and Co complex-functionalized blocks via living ROMP (**Figure 1.1B**).[33] They demonstrated that room temperature ferromagnetic materials can be obtained from such Co-containing block copolymers due to their self-assembly into nanodomains. In addition, they prepared block-random copolymers in which the random blocks contain both Co complex- and Fc-functionalized units (**Figure 1.1C**). This structure allows the magnetic properties of the resulting nanomaterial to be readily tuned by varying the molar ratio of Co to Fe units.[34]

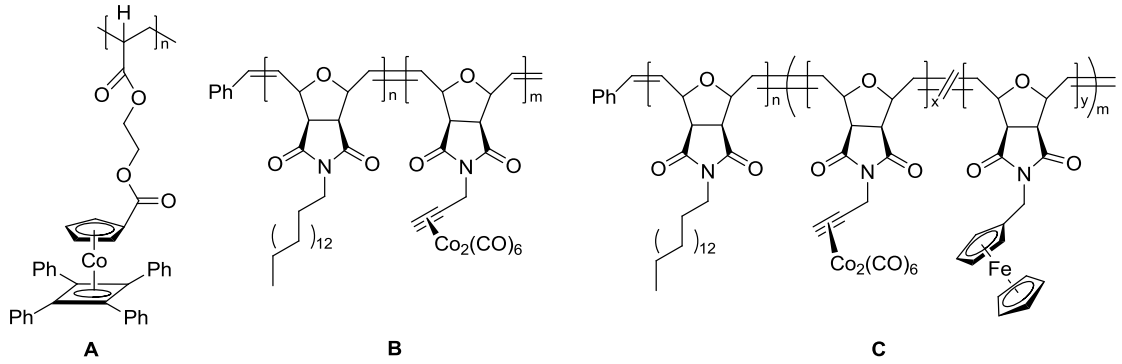

Figure 1.1 Structure of (A) $CpCo(C_4R_4)$-containing polymer, (B) $Co_2(CO)_6$-containing block copolymer and (C) $Co_2(CO)_6$-containing block-random copolymer.

1.2.1.3 Ruthenium-containing side-chain MCPs

Side-chain ruthenium(II) tris(bipyridine)-containing polymers have been reported via ROMP of monomers containing ruthenium(II) tris(bipyridine) (**Scheme 1.6**), which can be subsequently end-functionalized with biotin.[35, 36] These functionalized copolymers undergo self-assembly in water, forming star micelles composed of hydrophobic blocks containing ruthenium bipyridine in their core

and biotin at the periphery. These micelles are useful in luminescence detection and in signal amplification in biomolecules because of the presence of both the luminescent Ru-containing blocks and the molecular recognition biotin units in the single micelle.[37]

Scheme 1.6 Synthesis of side-chain ruthenium(II) tris(bipyridine) containing block copolymers and their end-biotinylation.[36]

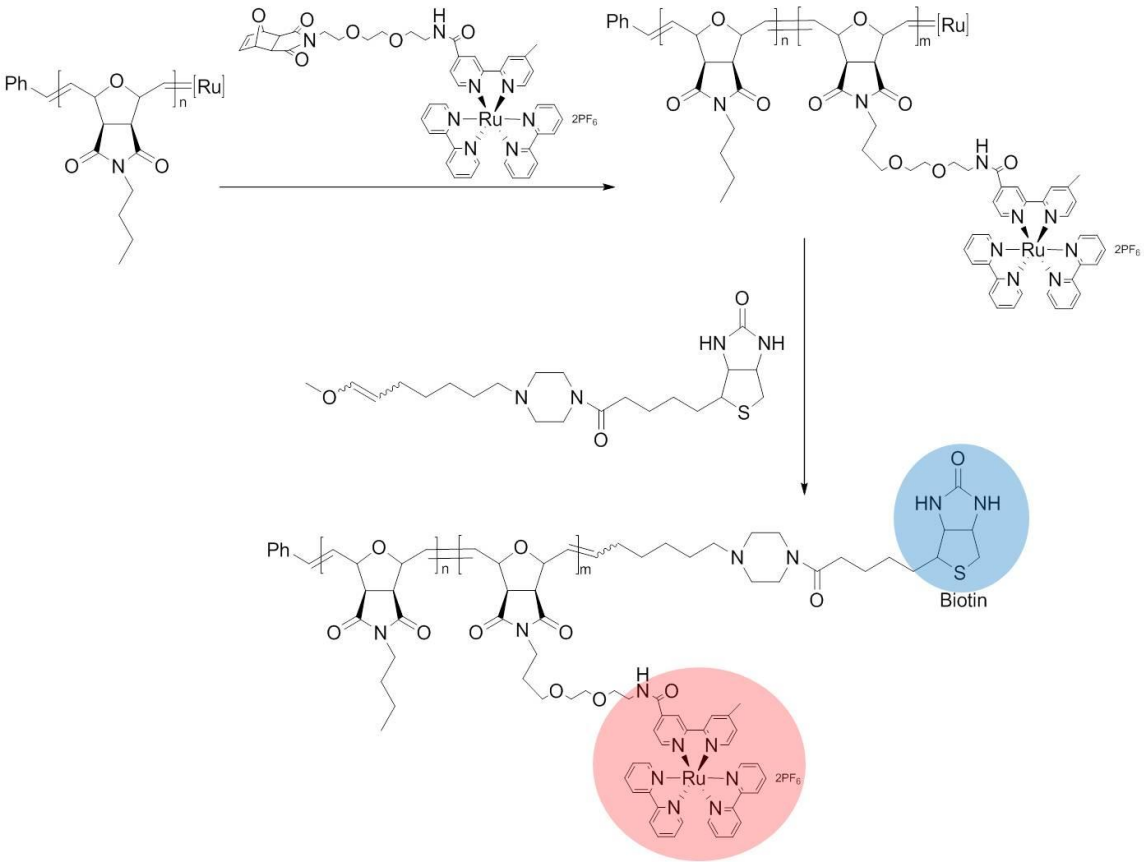

1.1.2 Side-chain MCPs prepared by post-polymerization treatment strategy

In this strategy, organic polymers with metal-binding functional groups are first synthesized, then

metal complexes are incorporated. Because of their ability to coordinate to different metals, pyridyl groups are widely employed in this strategy (**Figure 1.2**). For example, various Re-containing polymers were obtained via coordination of Re-containing complexes with pyridyl groups in the polymer chains (**Figure 1.2 A** and **B**).[38,39] In addition, pentacyanoferrate complexes were incorporated into the polymer side chain through the pyridyl groups (**Figure 1.2 C** and **D**). These pentacyanoferrate-coordinated block copolymers have been used for the controlled synthesis of soluble metal coordination nanoparticles.[40-42]

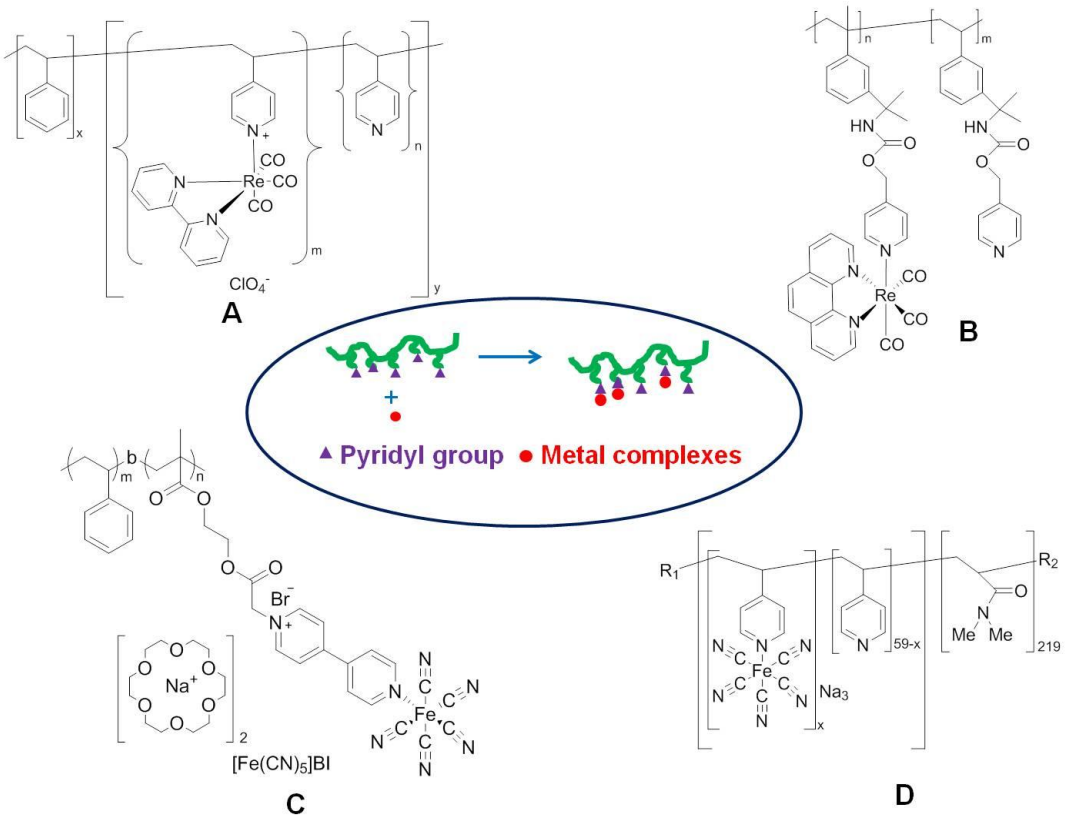

Figure 1.2 Side-chain MCPs synthesized by post-polymerization treatment strategy involving pyridyl groups.

1.2.3 Self-assembly of side-chain MCPs

The presence of metal elements may lead to unique self-assembly behaviors for metal-containing block copolymers. Wang and coworkers have reported block copolymers containing pendent dinuclear Ru complexes in their side chain.[43,44] These molecules are able to self-assemble into spherical micelles in acetonitrile with the Ru-containing blocks as the corona, and into vesicles in dioxane with the Ru-containing blocks as the vesicle walls (**Figure 1.3**). The luminescent properties of these nanostructures strongly depend upon the local environment of the Ru-containing blocks.[43,44] In another case, it was shown that side-chain cobaltocenium-containing block copolymers can self-assemble into vesicles in water and into nanotubes with monodispersed diameter in chloroform (**Figure 1.4**).[14]

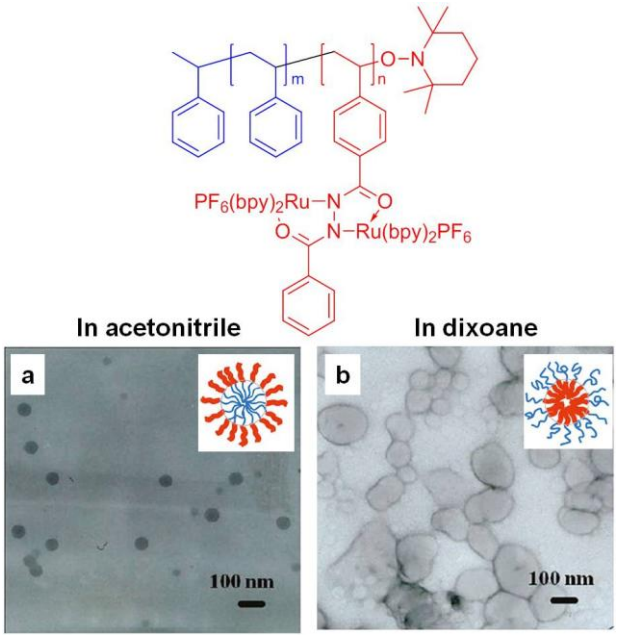

Figure 1.3 Structure of side-chain dinuclear ruthenium-containing block copolymer, and TEM images showing their self-assembled micellar structures (a) in acetonitrile and (b) in dioxane.[44]

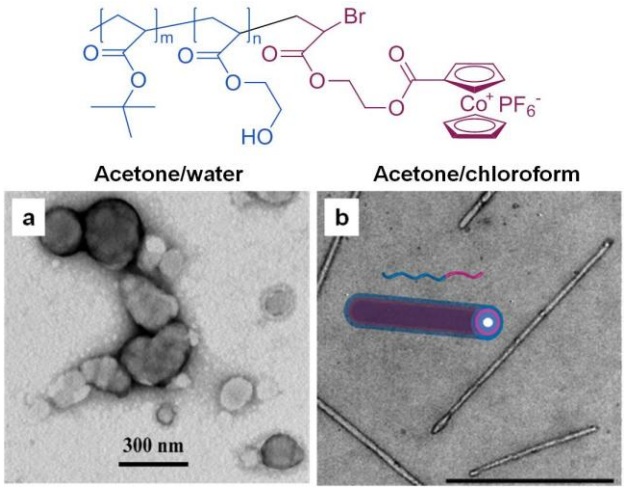

Figure 1.4 Structure of side-chain cobaltocenium-containing block copolymers, and TEM images showing their self-assembled micellar structures (a) in an acetone and water mixture and (b) in an acetone and chloroform mixture.[14]

1.3 Main-chain MCPs

Unlike side-chain MCPs, considerable synthetic challenges must be overcome to synthesize main-chain MCPs. For example addition polymerization, which tends to yield high molecular weight polymers, is virtually unexplored for main-chain MCPs, mainly because suitable monomers with metal-containing multiple bonds are lacking. Condensation polymerization requires high purity monomers, exact stoichiometry, and high reaction conversion to afford high molecular weight polymers, however this is not the case for difunctional organometallic species. In contrast, ROP reactions generally occur via a chain-growth mechanism and therefore represent a particularly desirable route for the preparation of high molecular weight main-chain MCPs.[11]

1.3.1 Synthesis of poly(metallocenes)

The major class of main-chain MCPs is poly(metallocenes). The early route for the preparation of poly(metallocenes) was condensation polymerization.[45] However most polymers obtained by this route had low molecular weights and were poorly defined.[45] To overcome these shortcomings, ROP became the primary focus for later investigations into the synthesis of poly(metallocenes).[11,45]

One key requirement for a classical ROP process is the presence of a strained ring in the monomers. Metallocenophanes, in which a single atom bridges the two cyclopentadienyl ligands, have strained-ring tilted structures and are therefore suitable for ROP. The first example of high molecular

weight poly(metallocenes) is the thermal ROP of silicon-bridged [1] ferrocenophanes with different substituents at the silicon or the cyclopentadienyl rings (**Scheme 1.7**),[46] leading to a wide range of poly(ferrrocenylsilanes) (PFS).[45] The structures of these polymers have been fully characterized using a range of techniques; their molecular weights lie in the 10^5- 10^6 g/mol range.[45]

Scheme 1.7 Thermal ROP of silicon-bridged ferrocenophane.[46]

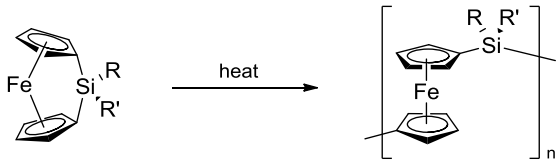

Although the thermal ROP is a convenient and effective polymerization technique, the molecular weights of the polymers are not controlled, and the polydispersity indices (PDIs) are fairly high (PDI=1.4-3.3).[45] Manners and coworkers reported the anionic ROP of ferrocenylsilanes using organolithium initiators.[47] Under stringent reaction conditions, the anionic ROP of extremely pure monomers is a living process.[12] PFS with controlled molecular weights (M_w) up to ca. 120,000 g/mol and very low PDIs (1.05-1.10) were prepared. Since the anionic ROP is living, functionalization of the ends of the polymer chain is facile, and the synthesis of block copolymers becomes feasible. Consequently, a number of PFS-based block copolymers have been reported, including PFS-polyisoprene (PFS-PI), PFS-poly(2-vinylpyridine) (PFS-P2VP), and PFS-poly(dimethylsiloxane) (PFS-PDMS).[48,49]

The living photolytic anionic ROP of silicon-bridged [1]ferrocenophane using the anionic initiator $Na[C_5H_5]$ under UV irradiation at 5 ℃ has been reported by Manners and coworkers.[50] After quenching the living homopolymers with methanol, H-capped PFS with a low PDI (< 1.1) was obtained. This method allows unprecedented photocontrolled ROP, which can provide access to new types of MCPs. This strategy has been employed for the synthesis of main-chain heterobimetallic block copolymers consisting of PFS and poly(cobaltoceniumethylene) ($[PCD]^+$) via **Scheme 1.8**.[51]

Scheme 1.8 Synthesis of heterobimetallic block copolymers through photocontrolled ROP (OTf^- = trifluoromethanesulfonate; triflate anion).[51]

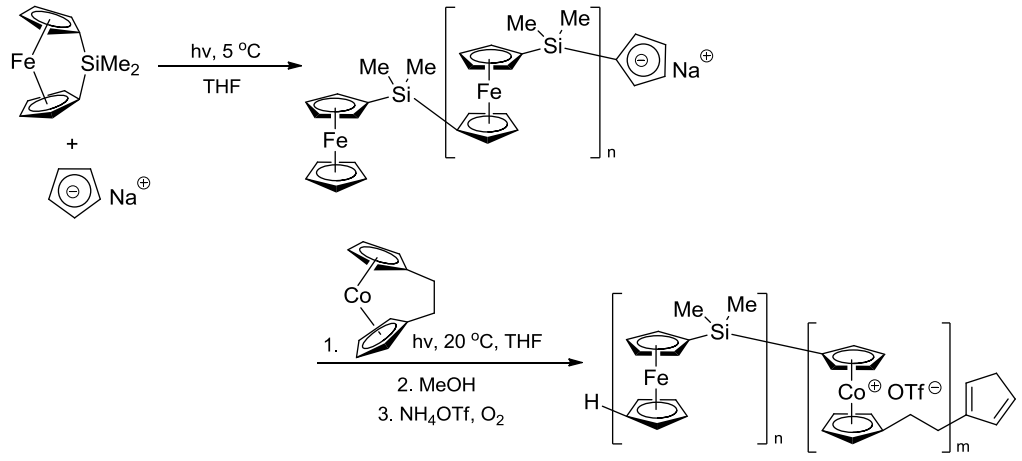

1.3.2 Living self-assembly of PFS block copolymers

Depending on the block ratio, PFS block copolymers tend to form elongated cylindrical or platelet micelles in a solvent selective for the organic block. The formation of these two extraordinary morphologies is driven by the crystallization of the PFS cores.[52] Upon addition of a second

PFS-containing block copolymer to the pre-existing PFS-containing micelles, homoepitaxial growth of the micelles occurs at specific crystal faces. This phenomenon possesses key features characteristic of a living polymerization, and led to the discovery of "living" supramolecular polymerization.[52] Various novel hierarchical architectures have been produced by employing living supramolecular polymerization, including centrosymmetric multiblock cylindrical comicelles (ABA, ABABA),[52] non-centrosymmetric (AB, ABC) multiblock cylindrical comicelles,[49] scarf micelles,[48] and lenticular platelet micelles[53] (**Figure 1.5**).

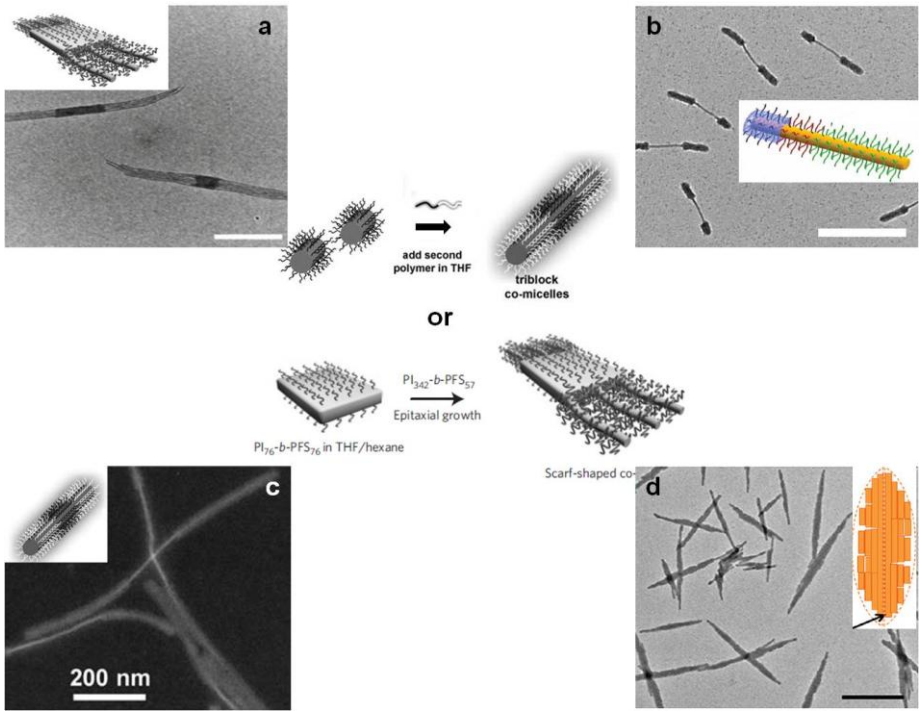

Figure 1.5 Different morphologies created by living supramolecular polymerization (a) scarf micelles, (b) non-centrosymmetric triblock comicelles, (c) centrosymmetric triblock comicelles and (d) lenticular platelet micelles.[48,49,52,53]

1.3.3 Synthesis of non-poly(metallocene) main-chain MCPs

Another type of main-chain MCPs produced by the ring-opening of 1-sila-3-metallacyclobutanes (**3**) was reported by Pannell and coworkers (**Scheme 1.9**).[54] In this work, 1-sila-3-metallacryclobutanes were formed by treating either **1** or **2** with lithium diisopropylamide (LDA), producing **3**. In **3**, the four-membered rings experience significant strain that provides the opportunity for ROP. Evaporation of the solvent from **3** generates the corresponding polymers **4**. The polymer structures have been characterized by various techniques. These polymers typically have either a bimodal molecular weight distribution or a high PDI (up to 6.3).

Scheme 1.9 Synthesis of organometallic polymers through the ring-opening of 1-sila-3-metallacyclobutane.[54]

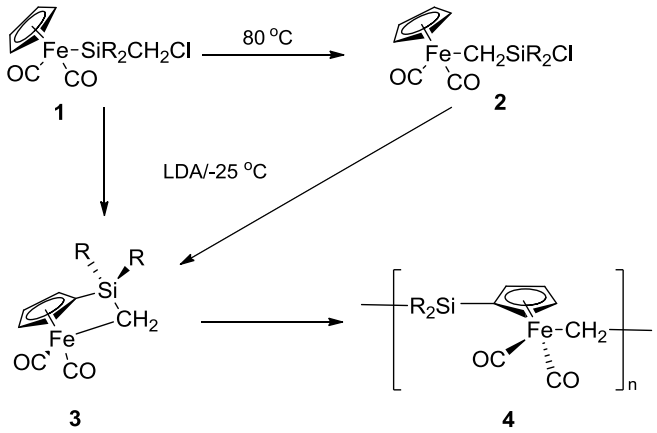

While side-chain MCPs can be prepared through various well-developed polymerization techniques, the synthesis of structure-defined and well-characterized main-chain MCPs is limited to ROP in the

presence of anionic initiators. Polymerizations involving anionic species require monomers with high purity and stringent experimental conditions. New techniques for synthesizing main-chain MCPs are thus highly desirable, and should be achievable upon taking advantage of well-developed synthetic organometallic chemistry and polymerization techniques. For example, the migratory insertion reaction is one of the well-studied organometallic reactions for that purpose.

1.4 Migratory insertion reaction (MIR)

Migratory insertion is a fundamental reaction in organometallic chemistry.[55] Organometallic complexes can react by insertion of an unsaturated ligand into an adjacent metal-ligand bond, followed by Lewis base binding to the vacant coordination site to generate the final products (**Scheme 1.10**).[55] The unsaturated ligand Y can be carbon monoxide, an olefin, an alkyne, a ketone, an aldehyde, or another related unsaturated species.[55] Classic cyclopentadienyl dicarbonyl iron alkyl complexes (FpR) undergo this class of reaction.[56,57] The reaction of FpR with nucleophilic ligands such as phosphine (PR_3) leads to air-stable iron complexes coordinated to phosphine and acyl ligands due to a migratory insertion process.[54,56]

Scheme 1.10 General reaction scheme for MIR.[55]

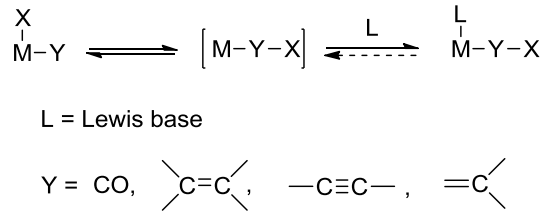

1.5 Research goal

The focus of my work was to develop a new polymerization technique for the synthesis of main-chain MCPs using MIR. To achieve this goal, an AB-type bifunctional monomer containing both cyclopentadienyl dicarbonyl iron (Fp) and diphenylphosphine (PPh_2) groups was designed. It was expected that these molecules would undergo intermolecular MIRs to produce polymers containing Fe in the main chain (**Scheme 1.11**).

Scheme 1.11 Reaction scheme for migratory insertion polymerization (MIP) of FpP.

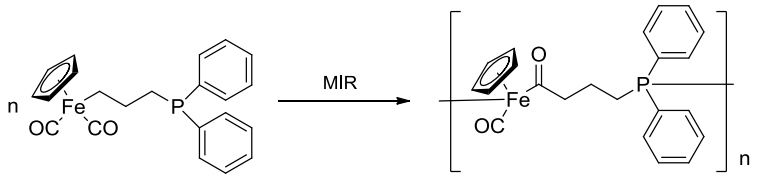

Chapter 2. Experimental

Materials

All experiments were performed under an atmosphere of dry nitrogen using standard Schlenk techniques or in a glovebox unless otherwise indicated. Tetrahydrofuran (THF) was freshly distilled under nitrogen from Na/benzophenone. Hexane, ethyl acetate (EA) and dichloromethane (DCM) were degassed using N_2, benzene and toluene were distilled over CaH_2 or 4 Å molecular sieves before use. Sodium (Na), 1-bromo-3-chloropropane ($BrCH_2CH_2CH_2Cl$), potassium (K), benzophenone and cyclopentadienyl iron dicarbonyl dimer (Fp_2) were purchased from Sigma-Aldrich (Oakville, ON, Canada). Chlorodiphenylphosphine (Ph_2PCl) was purchased from Tokyo Chemical Industry (TCI) (Portland, OR, USA). All chemicals were used as received unless otherwise indicated.

Instrumentation

Single crystals suitable for X-ray diffraction analysis were mounted onto the tips of glass fibers with thick oil and transferred immediately into the cold nitrogen gas stream of the diffractometer cryostat. X-ray data were collected using Mo Kα radiation at 200 K on a Bruker Kappa APEX II System (Madison, WI, USA). Structures were solved using direct methods and refined by full-matrix least squares on F_2 using the APEX2 package (v2012.4.0).[58]

Molecular weights and PDIs, M_w/M_n, were obtained by a Viscotek TDA-302 gel permeation

chromatography (GPC) at room temperature. THF at a flow rate of 1.0 mL/min was used as eluent on a system equipped with three PolyAnalytik mixed bed columns PAS-103-L, PAS-104-L and PAS-105-L (8mm (ID) × 300 mm (L) each, molecular weight range of 10^3-10^7 g/mol), refractive index, UV, viscosity, laser light scattering detectors. The data were analyzed with the Viscotek OmniSEC software package based on a universal calibration curves.

^{1}H, ^{31}P, and ^{13}C nuclear magnetic resonance (NMR) and Heteronuclear Multiple Quantum Coherence (HMQC) spectra were obtained on a Bruker Avance spectrometer (Milton, ON, Canada) at ambient temperature using appropriate solvents. H_3PO_4 was used as external reference for ^{31}P NMR analysis. The delays for HMQC were 1.5 s. The concentrations of NMR samples were ~ 5 mg/mL for ^{1}H and ^{31}P NMR and ~ 15 mg/mL for ^{13}C NMR and HMQC analysis. The NMR samples were prepared under N_2 atmosphere unless otherwise indicated.

Fourier transform infrared (FTIR) spectra were recorded as Nujol mulls between KBr plates using a Perkin Elmer Spectrum RX I FTIR system (Woodbridge, ON, Canada).

Ultraviolet-visible (UV-Vis) spectroscopy data were recorded on an Agilent 8453 UV-Vis spectrophotometer (Mississauga, ON, Canada) using a quartz cuvette with a path length of 1 cm. THF was used as the blank.

Positive ion nanoelectrospray (ESI) experiments were performed with a Waters/Micromass QTOF

Ultima Global mass spectrometer. Samples were infused at 1 L/min in dry acetonitrile. Typical operating conditions were: source temp=80^{o}C, capillary voltage=2.4 kV, cone voltage=60-160 V and mass resolution of 8000. MS/MS analysis was performed with argon as collision partner at a collision energy of 15 eV.

Differential scanning calorimetry (DSC) data were recorded using a differential scanning calorimeter (Q10, TA Instruments). Samples (~ 5 mg) were enclosed in an aluminum pan; an empty aluminum pan was used as the reference. Measurements were performed under a flow of N_2 (50 mL/min). Prior thermal history was eliminated by heating the samples from 25 ℃ to 150 ℃ (ramp: 10 ℃/min), then cooling back to –50 ℃ (ramp: 5 ℃/min). The measurement was performed by heating the samples from -50 ℃ to 150 ℃ (ramp: 10 ℃/min).

Thermal gravimetric analysis (TGA) was carried out on a TGA Q50 at a heating rate of 10 ℃/min. The samples were dried under vacuum at 50 ℃ overnight prior to TGA characterization.

2.1 Synthesis of sodium diphenylphosphide (Ph_2PNa)

A 100 mL Schlenk flask was charged with dry THF (60 mL). Sodium metal (2.07 g, 90 mmol) was cut into small pieces and added to the THF. Chlorodiphenylphosphine (5.38 mL, 30 mmol) was then added to the solution using a syringe. The reaction mixture was stirred for 3 days at 40 ℃. The solution turned dark orange, and a white precipitate was observed. This solution was used without

further purification. ^{31}P NMR (THF): -23 ppm.

2.2 Synthesis of (3-chloropropyl)diphenylphosphine ($Ph_2PCH_2CH_2CH_2Cl$)

2.2.1 Alkylation of Ph_2PH with $BrCH_2CH_2CH_2Cl$

Powdered KOH (1.12 g, 20 mmol) was added to a solution of Ph_2PH (1.50 g, 8 mmol), $BrCH_2CH_2CH_2Cl$ (1.88 g, 12 mmol) and triethylbenzylammonium chloride (TEBA) (0.20 g, 0.9 mmol) in CH_3CN (10 mL) with vigorous stirring at room temperature. The reaction mixture was heated at 70 ℃ for 1.5 h, the reaction mixture was allowed to cool to room temperature, and the solvent was removed under vacuum. Subsequently, the residue was heated at 60 ℃ for 2 h under vacuum to remove excess $BrCH_2CH_2CH_2Cl$. After cooling to room temperature, hexane was added to the residue, and the mixture was collected and washed with water (4 × 20 mL). The hexane solution was dried over Na_2SO_4 for ca. 1 h. The supernatant was transferred to another Schlenk flask via syringe, and the hexane was removed under vacuum at room temperature, yielding a colorless oil. Yield: 1.10 g (52 %). ^{1}H NMR ($CDCl_3$): 7.55 ppm, 7.28 ppm (10H, $C_6\boldsymbol{H_5}$), 3.60 ppm (*t*, 2H, $C\boldsymbol{H_2}Cl$), 2.20 ppm (*t*, 2H, $C\boldsymbol{H_2}P$) and 1.92 (*m*, 2H, $CH_2C\boldsymbol{H_2}CH_2$). ^{31}P NMR ($CDCl_3$): -15.4 ppm.

2.2.2 Alkylation of Ph_2PNa with $BrCH_2CH_2CH_2Cl$

A 250 mL Schlenk flask was charged with a solution of $BrCH_2CH_2CH_2Cl$ (7.87 g, 50 mmol)

dissolved in dry THF (50 mL). To this solution, Ph_2PNa in THF solution (60 mL, 30 mmol) was added dropwise at 0 ℃ with stirring. This mixture was allowed to warm to room temperature and stirred overnight, yielding a colorless solution with a white precipitate. After the reaction, the solvent was removed under vacuum and the residue was heated at 60 ℃ for ca. 2 h in vacuo to remove excess $BrCH_2CH_2CH_2Cl$. The crude product was dissolved in hexane and filtered through silica gel. The filtrate was collected and the solvent was removed under vacuum at room temperature, yielding a colorless oil. Yield: 5.52 g (70 %). ^{1}H NMR ($CDCl_3$): 7.55 ppm, 7.28 ppm (10H, $C_6\boldsymbol{H_5}$), 3.60 ppm (*t*, 2H, $C\boldsymbol{H_2}Cl$), 2.20 ppm (*t*, 2H, $C\boldsymbol{H_2}P$) and 1.92 (*m*, 2H, $CH_2C\boldsymbol{H_2}CH_2$). ^{31}P NMR ($CDCl_3$): -15.4 ppm.

2.3 Synthesis of cyclopentadienyl dicarbonyl iron metalate (Fp anion)

2.3.1 Reduction with $K[HBEt_3]$

Cyclopentadienyl dicarbonyl iron dimer (Fp_2) (0.50 g, 1.4 mmol) was dissolved in THF (24 mL) in a 100 mL Schlenk flask, and the mixture was refluxed for 0.5 h. After cooling to room temperature, $K[HBEt_3]$ in THF solution (1 M) (5 mL, 5.0 mmol) was added. After the reaction mixture was stirred at room temperature for 1 h, $Ph_2PCH_2CH_2CH_2Cl$ (0.73 g, 2.8 mmol) was added to the solution and stirred for 2 h, followed by filtration through Celite (Imerys Minerals California, Inc.). The filtrate was collected and the solvent was removed under vacuum, yielding a red-brown viscous liquid. The red-brown viscous liquid was separated by chromatography on a silica gel column, and eluted sequentially with hexane/EA (8:2 v/v), hexane/EA (5:5 v/v), EA and THF, giving seven fractions.

NMR characterization of selected band is included in Appendix A5.

2.3.2 Reduction with Na metal

A Na dispersion was first prepared by charging a 100 mL Schlenk flask equipped with a reflux condenser with Na metal (0.50 g, 22 mmol) and toluene (30 mL). The mixture was heated to reflux in an oil bath until the Na melted. The condenser was then removed, the flask was capped with a glass stopper, and removed from the oil bath. The flask was then shaken vigorously to break the Na into very small globules, and the majority of the toluene (ca. 90 %) was removed under vacuum. Then, Fp_2 (0.30 g, 0.85 mmol) and THF (24 mL) were added, and the mixture was refluxed for 6 h. After cooling to room temperature, the NaFp/THF solution was transferred to another Schlenk flask via syringe. To this solution, a solution of $Ph_2PCH_2CH_2CH_2Cl$ (0.75 g, 2.9 mmol) in THF (5 mL) was added at 0 ℃, and the reaction mixture was stirred at room temperature overnight. THF was then removed under vacuum and the remaining residue was dissolved in hexane. The supernatant was transferred out, concentrated, and separated by chromatography on a silica gel column. The column was eluted with a solvent mixture composed of hexane/EA (9:1 v/v), resulting in a light yellow band that was characterized mainly as the starting material, $Ph_2PCH_2CH_2CH_2Cl$. No target product was obtained.

2.3.3 Reduction with Na/Hg amalgam

THF (10 mL) and Fp_2 (0.50 g, 1.4 mmol) were added to Na metal (0.19 g, 8.2 mmol) in a 1.2 % Na/Hg amalgam, the reaction mixture was stirred for 40 min at room temperature, and the amalgam was allowed to settle. The resulting NaFp/THF solution was transferred to another Schlenk flask, $Ph_2PCH_2CH_2CH_2Cl$ (0.75 g, 2.8 mmol) was added at 0 ℃, and the reaction mixture was stirred at room temperature for 2 h. The solution was then concentrated and purified by chromatography on a silica gel column eluting with hexane:EA (9:1 v/v). The resulting yellow band was characterized, and contained target molecules and starting material $Ph_2PCH_2CH_2CH_2Cl$. ^{1}H NMR (DMSO-d_6): 7.35 ppm, 7.32 ppm (10H, $C_6\boldsymbol{H_5}$), 4.87 ppm (*s*, 5H, $C_5\boldsymbol{H_5}$), 2.07 ppm (*s*, 2H, $PC\boldsymbol{H_2}$), 1.46 ppm (*s*, 4H, $FeC\boldsymbol{H_2}C\boldsymbol{H_2}$), 3.60 ppm (*t*, 2H, $C\boldsymbol{H_2}Cl$), 2.20 ppm (*t*, 2H, $C\boldsymbol{H_2}P$) and 1.92 ppm (*m*, 2H, $CH_2C\boldsymbol{H_2}CH_2$). ^{31}P NMR (DMSO-$d_6$): -14.5 ppm, -14.6 ppm.

2.3.4 Reduction with potassium benzophenone ketyl

Potassium benzophenone ketyl was prepared by stirring benzophenone (4.90 g, 27 mmol) and small pieces of K metal (0.97 g, 25 mol) in dry THF (50 mL). Upon mixing, the mixture immediately turned a dark blue. The mixture was stirred overnight to ensure complete solvation of the K metal. To this solution, Fp_2 (4.60 g, 13 mmol) dissolved in dry THF (20 mL) was added with vigorous stirring. Within several minutes, the solution turned from deep blue to red-brown, and an orange precipitate formed. The mixture was stirred for ca. 1 h at room temperature, and the THF was removed under

vacuum. The resulting residue was washed with toluene (or benzene) several times to remove benzophenone and unreacted Fp_2. The supernatant was removed via cannula, and the residue was dried under vacuum at room temperature, yielding an orange powder. Yield: 3.52 g (65 %).

2.4 Synthesis of cyclopentadienyl(dicarbonyl)(diphenylphosphinopropyl)iron (FpP)

A solution of $Ph_2PCH_2CH_2CH_2Cl$ (1.44 g, 5.5 mmol) in THF (5 mL) was added to a suspension of FpK (1.00 g, 4.6 mmol) in THF (20 mL) at 0 ℃ with stirring, and the mixture was stirred at room temperature. During stirring, the orange suspension gradually turned brown; after 1.5 h, the brown solution was filtered through Celite to remove KCl. The red-brown filtrate was collected and the solvent was removed under vacuum, resulting in a dark red-brown oil. This red-brown oil was dissolved in a minimum volume of hexane/DCM (3.5:1, v/v) and the solution was purified by chromatography on a silica gel column. Elution with hexane/DCM (3.5:1, v/v) resulted in four bands. The first band was eluted as a yellow fraction which was characterized as cyclopentadienyl-(carbonyl)[3-(diphenylphosphanyl-κP)prop-1-yl]iron (cyclic FpP5, formed by an intramolecular cyclization reaction, see **Sec 2.5**), the second colorless band was characterized via ^{1}H NMR as the $Ph_2PCH_2CH_2CH_2Cl$ starting material. The third fraction gave a bright yellow band, which was found to be the product, FpP. The fourth brown band near the top of the column contained Fp_2. Yield 1.10 g (60 %). ^{1}H NMR (DMSO-d_6): 7.35 ppm, 7.32 ppm (10H, $C_6\boldsymbol{H_5}$), 4.87 ppm (*s*, 5H, $C_5\boldsymbol{H_5}$), 2.07 ppm (*s*, 2H, $PC\boldsymbol{H_2}$), 1.46 ppm (*s*, 4H, $FeC\boldsymbol{H_2}C\boldsymbol{H_2}$). ^{1}H NMR ($C_6D_6$): 7.61 ppm, 7.20 (10H, $C_6\boldsymbol{H_5}$), 4.03 ppm (*s*, 5H, $C_5\boldsymbol{H_5}$), 2.25 ppm (*t*, 2H, $PC\boldsymbol{H_2}$), 1.80 ppm (*m*, 2H, $CH_2C\boldsymbol{H_2}CH_2$), 1.64 ppm (*t*, 2H, $FeC\boldsymbol{H_2}$). ^{13}C

NMR (DMSO-d_6): 5.1 ppm (*d*, Fe***C***H_2), 32.6 ppm (*d*, CH_2***C***H_2CH_2), 34.4 ppm (*d*, P***C***H_2), 86.3 ppm (***C***$_5H_5$), 128.9 ppm, 132.7 ppm, 139.4 ppm (***C***$_6H_5$), 218.7 ppm (Fe***C***≡O). ^{31}P NMR (C_6D_6): -14.4 ppm. ^{31}P NMR (DMSO-d_6): -14.6 ppm. FTIR: 2004 cm^{-1}, 1952 cm^{-1} (terminal CO stretch). m/z 405.1 ($M+H^+$).

2.5 Synthesis of cyclopentadienyl(carbonyl)[3-(diphenylphosphanyl-κP)prop-1-yl]iron (cyclic FpP5)

FpP was dissolved in THF (10 mg/mL), and the reaction mixture was heated at 70 ℃ for 2 h (or at room temperature for 7 days) in the light. After cooling to room temperature the solvent was removed under vacuum, yielding a clear orange oil. The orange oil was separated by chromatography on a silica gel column using hexane/EA (10:1 v/v) to yield an orange oil. This oil was recrystallized from hexane at -49 ℃ to yield orange crystals. Yield: 70 %. ^{1}H NMR ($CDCl_3$): 7.76 ppm, 7.49 ppm, 7.33 ppm and 7.15 ppm (10H, C_6***H***$_5$), 4.21 ppm (*s*, 5H, C_5***H***$_5$), 2.50 ppm (*m*, 1H, PC***H***$_2$), 2.30 ppm (*m*, 1H, PC***H***$_2$), 2.10 ppm, (*m*, 1H, CH_2C***H***$_2CH_2$), 1.20 ppm (*m*, 1H, CH_2C***H***$_2CH_2$), 2.0 ppm (*m*, 2H, FeC***H***$_2$). ^{13}C NMR (Dept-135, $CDCl_3$): 36 ppm (*d*, P***C***H_2), 31 ppm (*d*, CH_2***C***H_2CH_2), 21 ppm (*d*, Fe***C***H_2). 82.6 ppm (*s*, ***C***$_5H_5$), 134 ppm, 130 ppm and 128 ppm (***C***$_6H_5$). ^{31}P NMR ($CDCl_3$): 109 ppm.

2.6 Synthesis of cyclopentadienyl(carbonyl)[(4-diphenylphosphanyl-κP)butanoyl]iron (cyclic FpP6)

FpP was dissolved in THF (10 mg/mL), and the reaction mixture was heated at 70 ℃ for 2 h in the dark (covered by aluminum foil). After cooling to room temperature, the solvent was removed under vacuum, yielding a yellow oil. The yellow oil was separated by chromatography on a silica gel column using hexane/EA (2.5:1 v/v). The resulting oil was recrystallized from DCM/hexane (1:5 v/v) at -49 ℃, yielding yellow crystals. Yield: 55 %. ^{1}H NMR ($CDCl_3$): 7.62 ppm, 7.48 ppm (10H, $C_6\boldsymbol{H_5}$), 4.52 ppm (*s*, 5H, $C_5\boldsymbol{H_5}$), 2.84 ppm (*t*, 1H, COC$\boldsymbol{H_2}$), 2.33 ppm (*m*, 1H, COC$\boldsymbol{H_2}$), 2.50 ppm (*m*, 1H, PC$\boldsymbol{H_2}$), 2.33 ppm (*m*, 1H, PC$\boldsymbol{H_2}$), 1.91 ppm (*m*, 1H, $CH_2C\boldsymbol{H_2}CH_2$), 1.30 ppm (*m*, 1H, $CH_2C\boldsymbol{H_2}CH_2$). ^{13}C NMR (Dept-135, $CDCl_3$): 68 ppm (*s*, CO$\boldsymbol{C}H_2$), 29 ppm (*d*, P$\boldsymbol{C}H_2$), 21 ppm (*b*, Fe$\boldsymbol{C}H_2$). 82.6 ppm (*s*, $\boldsymbol{C_5}H_5$), 134 ppm, 130 ppm and 128 ppm ($\boldsymbol{C_6}H_5$). ^{31}P NMR ($CDCl_3$): 70 ppm.

2.7 Synthesis of poly(cyclopentadienylcarbonyldiphenylphosphinobutanoyliron) (PFpP)

In a typical experiment, FpP (0.5 g, 1.2 mmol) was heated in a 50 mL Schlenk flask at 70 ℃ or 75 ℃ for a designated time, and the polymerization was terminated by cooling to room temperature. This crude product was purified by dissolution in a minimum volume of THF (or DCM) and precipitated in hexane at room temperature. The precipitate was collected by filtration and dried under vacuum at room temperature. ^{1}H NMR (DMSO-d_6): 7.8-7.1 ppm (*b*, 10H, $C_6\boldsymbol{H_5}$), 4.4-4.2 ppm (*b*, 5H, $C_5\boldsymbol{H_5}$), 2.78-2.60 ppm (*b*, 1H, COC$\boldsymbol{H_2}$), 2.47-2.17 ppm (*b*, 1H, COC$\boldsymbol{H_2}$), 2.13-1.89 ppm (*b*, 2H, C$\boldsymbol{H_2}$P), and

1.32-0.74 ppm (*b*, 2H, $CH_2C\boldsymbol{H_2}CH_2$). ^{13}C NMR (DMSO-d_6): 20 ppm (*s*, $CH_2\boldsymbol{C}H_2CH_2$), 28 ppm (*d*, $P\boldsymbol{C}H_2$), 66 ppm (*s*, $\boldsymbol{C}H_2C{=}O$), 84 ppm, 86 ppm ($\boldsymbol{C_5}H_5$), 127 ppm, 128 ppm, 129 ppm, 130 ppm, 132 ppm ($\boldsymbol{C_6}H_5$), 220 ppm, 217 ppm (*d*, *s*, $\boldsymbol{C}{\equiv}O$), and 274 ppm (s, $CH_2\boldsymbol{C}{=}O$). ^{31}P NMR ($CDCl_3$): 73.4 ppm, 72.3 ppm, and -13.6 ppm. FTIR: 1910 cm^{-1} (terminal CO stretch), 1600 cm^{-1} (ketonic CO stretch).

Chapter 3. Results and discussion

3.1 Synthesis of $Ph_2PCH_2CH_2CH_2Cl$

Two routes have been successfully employed for the synthesis of $Ph_2PCH_2CH_2CH_2Cl$: 1) alkylation of Ph_2PH with $BrCH_2CH_2CH_2Cl$ in the presence of KOH,[59] and 2) alkylation of Ph_2PNa with $BrCH_2CH_2CH_2Cl$ (**Scheme 3.1**).[60] During these reactions, phosphorus in the product is partially oxidized; the oxidized phosphine species can then be removed from the product via filtration through silica gel using hexane as eluent. As the Ph_2PH used in the first route is expensive and the second route is experimentally simpler and has a higher yield, the latter route was used in this study.

Scheme 3.1 Synthesis of $Ph_2PCH_2CH_2CH_2Cl$. 1) Alkylation of Ph_2PH with $BrCH_2CH_2CH_2Cl$ and 2) alkylation of Ph_2PNa with $BrCH_2CH_2CH_2Cl$.

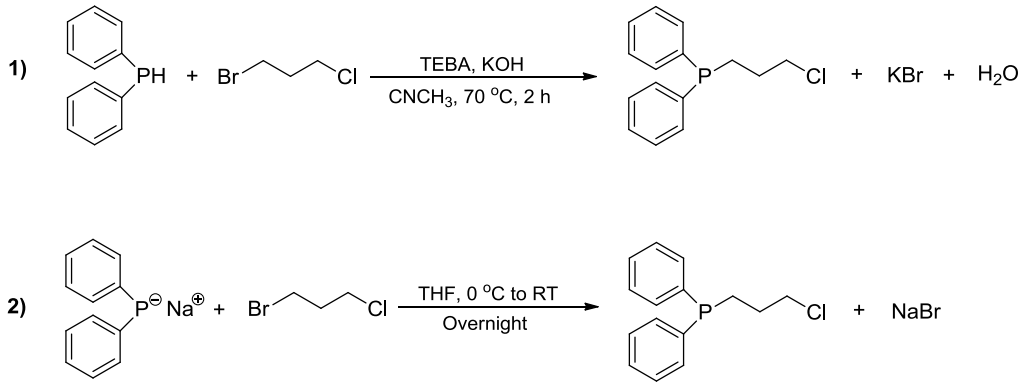

The product was characterized using ^1H and ^{31}P NMR spectroscopies. The ^1H NMR spectrum is shown in **Figure 3.1.** As shown, the triplet signals at 3.60 ppm and 2.20 ppm were attributed to the protons in CH_2 adjacent to chlorine and to the diphenylphosphine group, respectively. The multiplet

peak at 1.90 ppm was associated with the CH_2 protons in the middle of the propyl spacer. The peak at 7.55-7.28 ppm belonged to the phenyl group protons. The integration ratio of this peak to that at 3.60 ppm (CH_2 next to Cl) was 5:1, which was consistent with the number of protons in the designated structure. In addition, the ^{31}P NMR spectrum of the product (**Figure 3.2**) displayed a sharp peak at -15.4 ppm, corresponding to the diphenylphosphine group in the product.[59] The NMR analysis indicated the formation of $Ph_2PCH_2CH_2CH_2Cl$.

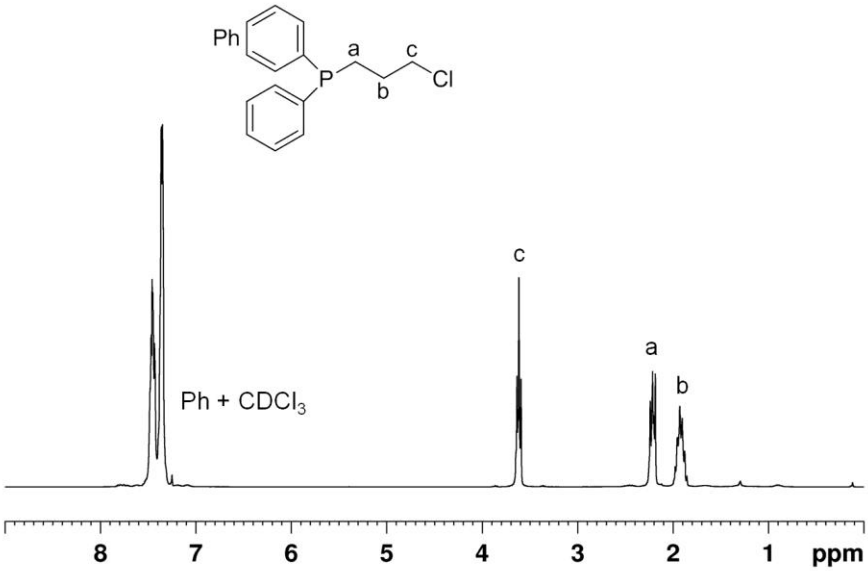

Figure 3.1 ^1H NMR spectrum of $Ph_2PCH_2CH_2CH_2Cl$ in $CDCl_3$.

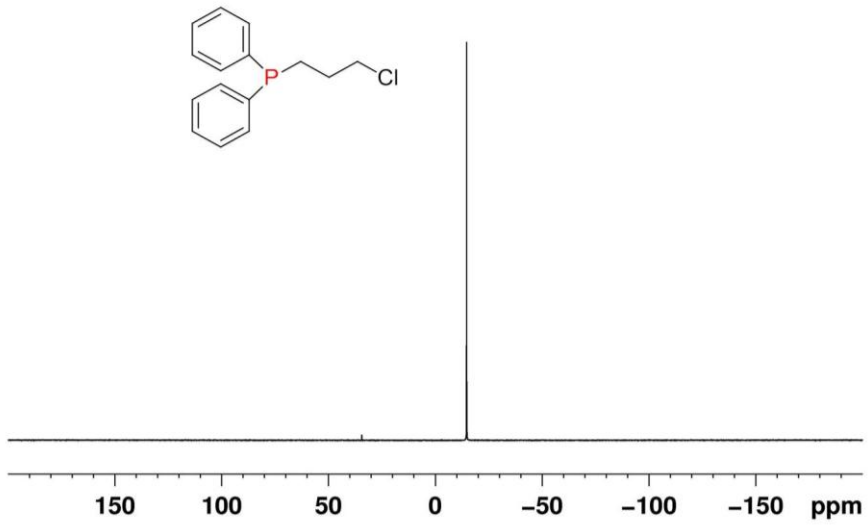

Figure 3.2 ^{31}P NMR spectrum of $Ph_2PCH_2CH_2CH_2Cl$ in $CDCl_3$.

3.2 Synthesis of Fp anion

The Fp anion was prepared by the reduction of cyclopentadienyl dicarbonyl iron dimer (Fp_2) according to standard literature procedures.[61-64] Different reducing agents including $K[HBEt_3]$,[61] sodium metal,[62] Na/Hg amalgam,[63] and potassium benzophenone ketyl[64] were used for the reduction reaction (**Scheme 3.2**). First, $K[HBEt_3]$ was used to reduce the Fp_2 dimer (**Scheme 3.2A**), and the resulting anion was reacted with $Ph_2PCH_2CH_2CH_2Cl$. However this reaction gave a number of unknown products, leading to difficulty in separation and characterization. Second, the Na metal was refluxed with Fp_2 for reduction (**Scheme 3.2B**). The yield of the Fp anion was low, probably due to the heterogeneous nature of the reaction system. To overcome this problem, the sodium in mercury amalgam (Na/Hg amalgam) was employed as the reducing agent (**Scheme 3.2C**), and the resulting Fp

anion was reacted with $Ph_2PCH_2CH_2CH_2Cl$. By this method, the target molecules were obtained. This method is simple, rapid, and widely used.[57] However the low solubility of alkali metals in mercury requires handling large quantities of mercury, which is toxic and requires extra care.[57] Finally, we used potassium benzophenone ketyl to reduce Fp_2 (**Scheme 3.2D**), which provided a convenient means of synthesizing the Fp anion. Furthermore, the FpK orange powder produced by this method is readily isolated, is stable under inert atmosphere, and can be used as a stoichiometric reagent. For these reasons, the potassium benzophenone ketyl method was employed in this study.

Scheme 3.2 Synthesis of Fp anion using A) $K[HBEt_3]$, B) Na metal, C) Na/Hg amalgam, and D) potassium benzophenone ketyl as reducing agents.

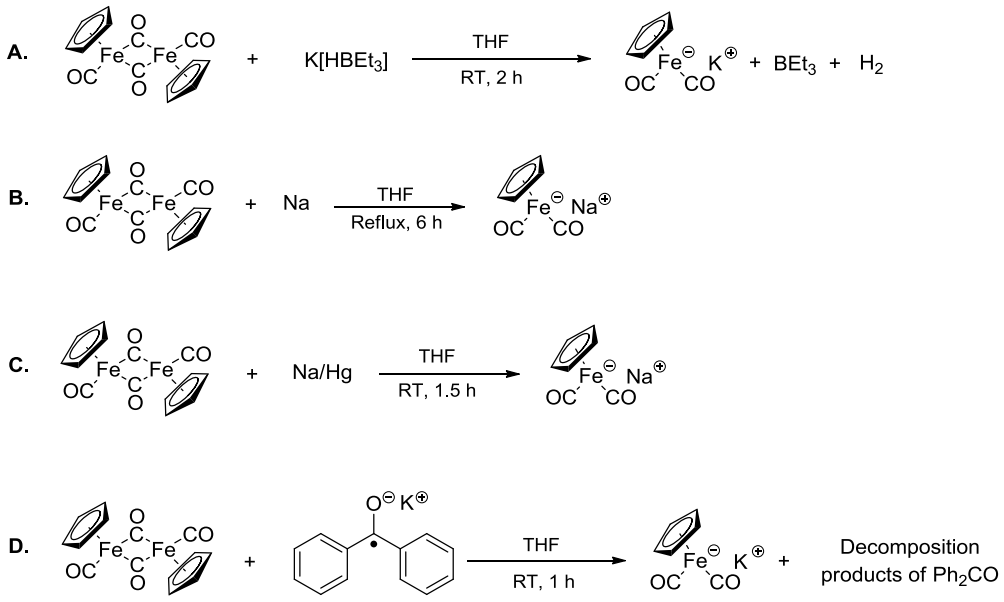

3.3 Synthesis of FpP

The FpP was synthesized by the substitution reaction between FpK and $Ph_2PCH_2CH_2CH_2Cl$, in which the chlorine is replaced by the Fp to form a metal-carbon bond (**Scheme 3.3**).[65,66] The resulting product was collected as a transparent yellow oil and characterized using FTIR, ^{1}H NMR, ^{31}P NMR, ^{13}C NMR and UV-Vis spectroscopies.

Scheme 3.3 Synthesis of FpP.

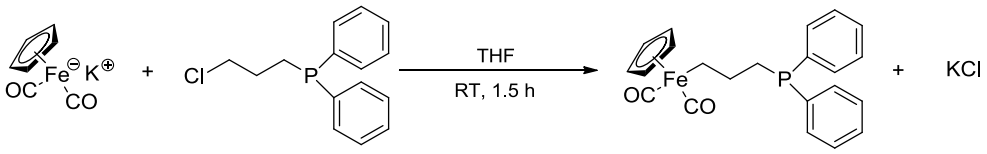

3.3.1 FpP structure characterization

FTIR spectroscopy was first used for the characterization. As shown in **Figure 3.3**, the resulting compound revealed two absorption frequencies for CO at 1952 cm^{-1} and 2004 cm^{-1}. This suggested that only terminal CO (C≡O) existed in the compound.[56]

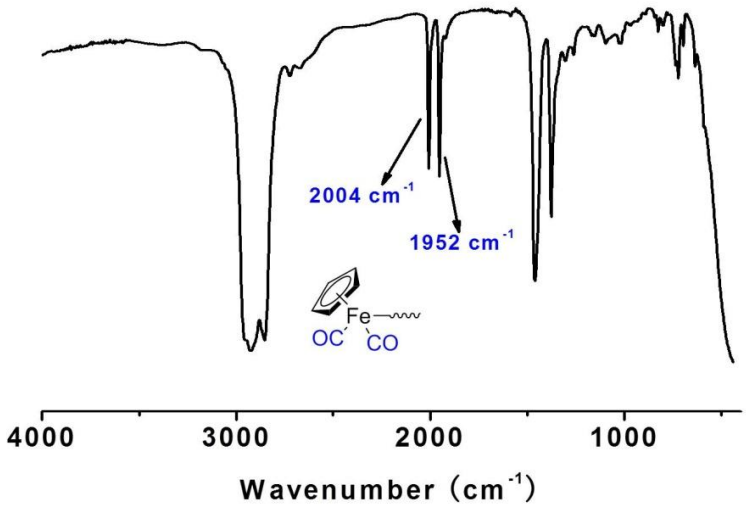

Figure 3.3 FTIR spectrum of FpP.

^{1}H NMR analysis was carried out in different solvents to assign the signals clearly. The ^{1}H NMR spectrum using DMSO-d_6 as solvent is shown in **Figure 3.4a**. The signal at 4.88 ppm was assigned to the Cp protons and the signal at 7.40-7.28 ppm was attributed to phenyl group protons.[65,67] The integration ratio of the Cp peak to the phenyl group peak was 1:2, corresponding to the number of protons in the desired structure. In addition, the peak at 3.60 ppm, which was due to the CH_2 adjacent to Cl in $Ph_2PCH_2CH_2CH_2Cl$ (**Figure 3.1**) disappeared, and a peak at 1.46 ppm was observed, which suggested that the Cl reacted and an Fe-C bond was formed.[67] The signal of the CH_2 protons in the middle of the propyl spacer also appeared at 1.46 ppm, which was at the same position as the CH_2 protons next to Fe. The signal at 2.10 ppm was due to the CH_2 protons next to the dipentylphosphine group. The integration ratio of the signals at 1.46 ppm and at 2.10 ppm was 2:1, corresponding to the

number of protons in the expected structure. NMR analysis using C_6D_6 as solvent was also carried out, and the result is shown in **Figure 3.4b**. The signals upfield are clearly observed and well-separated. The triplet peak at 2.25 ppm was attributed to the CH_2 protons next to phosphorus, the multiple peak at 1.80 ppm was assigned to the CH_2 protons in the middle of the propyl spacer, and a triplet peak attributed to the CH_2 proton adjacent to Fe was observed at 1.64 ppm.[67] The signal at 4.0 ppm was attributed to the Cp protons, while the signals at 7.6 ppm and 7.3 ppm were caused by phenyl group protons.[67] The compound was also characterized using ^{31}P NMR (**Figure 3.5**). The peak at -14.7 ppm correspond to the phosphine group in the desired molecule. The compounds were also studied using ^{13}C NMR. As shown in **Figure 3.6**, the peak at 217 ppm was attributed to the terminal CO group and the peak at 85 ppm was assigned to the Cp ring.[56] The signals at 128 ppm, 132 ppm and 139 ppm were caused by the phenyl ring. Three doublet peaks at 36 ppm, 34 ppm, and 5.1 ppm arose from the three carbons in the propyl spacer, as shown in **Figure 3.6**.[56] The multiplicity of these peaks was caused by the coupling with phosphors in the compound. NMR analysis indicated that the molecule FpP was successfully synthesized.

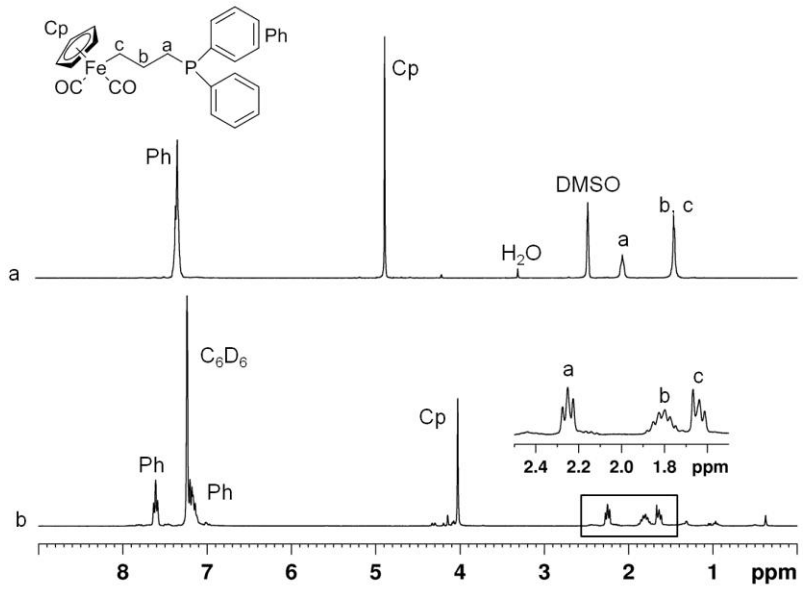

Figure 3.4 ^{1}H NMR spectra of FpP (a) in DMSO-d_6 and (b) in C_6D_6.

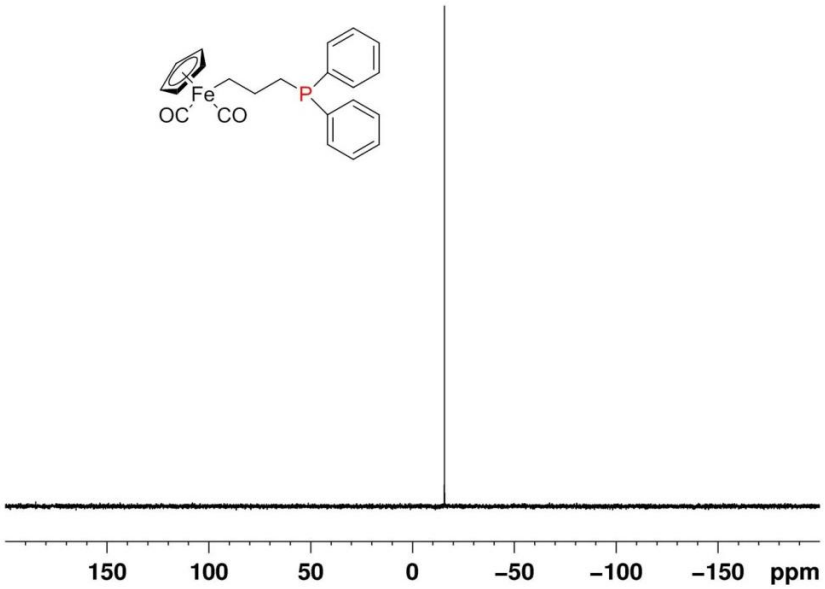

Figure 3.5 ^{31}P NMR spectrum of FpP in DMSO-d_6.

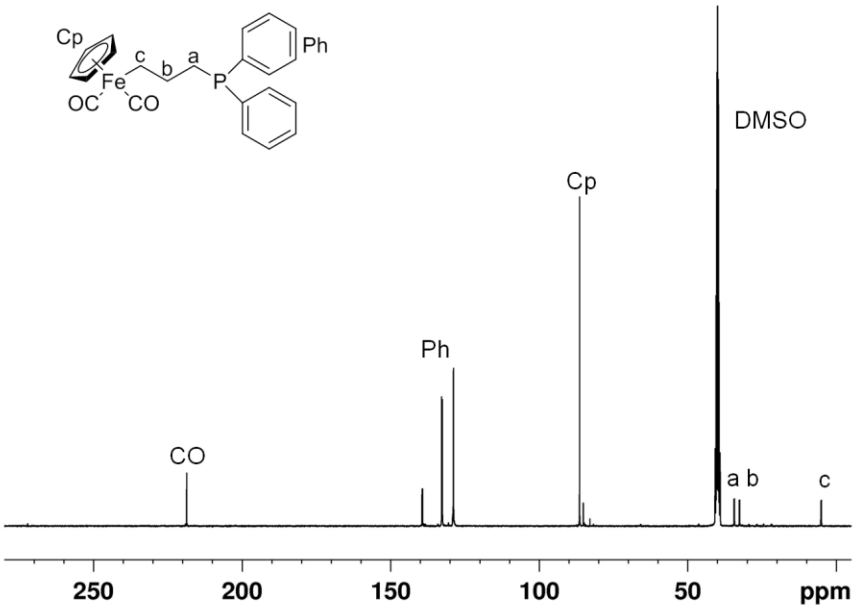

Figure 3.6 ^{13}C NMR spectrum of FpP in DMSO-d_6.

FpP was also characterized using UV-Vis spectroscopy (**Figure 3.7**). The measurement was carried out in THF with an FpP concentration of 2 mmol/L. The compound showed an absorption between 320 nm and 450 nm (λ_{max} = 346 nm).[51]

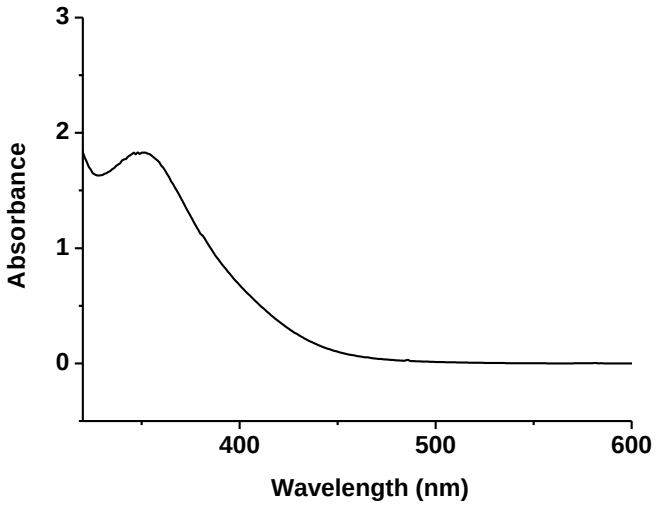

Figure 3.7 UV-Vis spectrum of FpP in THF (2 mmol/L).

3.3.2 Cyclization reactions of FpP

The FpP underwent intramolecular cyclization reactions in organic solvents, resulting in two ring structures, cyclopentadienyl(carbonyl)[3-(diphenylphosphanyl-κP)prop-1-yl]iron (cyclic FpP5) formed via a release of CO, and cyclopentadienyl(carbonyl)[(4-diphenylphosphanyl-κP)butanoyl]iron (cyclic FpP6), formed via an MIR (**Scheme 3.4**).

Scheme 3.4 Cyclization reactions of FpP.

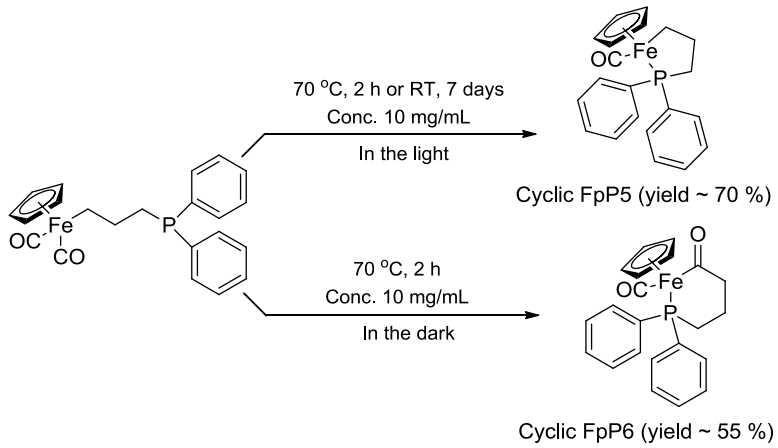

3.3.2.1 Synthesis and characterization of cyclic FpP5

The cyclic FpP5 was formed by heating a dilute solution of FpP (10 mg/mL) at 70 ℃ for 2 h or leaving the solution at room temperature for 7 days in the light.[68] The structure of cyclic FpP5 was confirmed using single-crystal X-ray diffraction (XRD) using a sample obtained by recrystallization of cyclic FpP5 at -49 ℃ in hexane. The compound crystallized in the monoclinic $P2_1/c$ space group. As shown in **Figure 3.8**, the phosphorus is coordinated to the Fe center, leading to a five-membered ring.

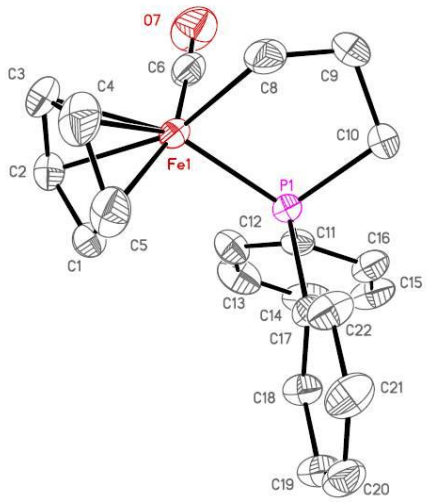

Figure 3.8 Crystal structure of cyclic FpP5 with thermal ellipsoids (50% probability level). Hydrogen atoms are omitted for clarity.

The ^{31}P NMR spectrum of cyclic FpP5 is shown in **Figure 3.9**. As shown, this compound exhibited a single peak at 109 ppm. Cyclic FpP5 was also characterized using ^{1}H NMR spectroscopy, shown in **Figure 3.10**. The Cp signal occurred at 4.2 ppm; this peak underwent a 0.6 ppm upfield shift as compared to that for FpP, which provided evidence for coordination of phosphorus to the metal center. The phenyl signals were found at 7.8-7.1 ppm. The integration ratio of the Cp and phenyl peaks was 2:1, corresponding to the number of protons in cyclic FpP5. The peaks at 2.5-1.3 ppm were attributed to the CH_2 protons in the propyl spacer; these protons gave rise to complicated signals at this region. To assign these peaks, an ^{1}H-^{13}C HMQC 2D NMR experiment was performed (**Figure 3.11)**. The proton signals appearing at 2.50 ppm and 2.30 ppm were correlated to the C atom adjacent to the P atom, whose signal occurred at 36 ppm in ^{13}C NMR. The protons at 2.0 ppm were connected to the C atom whose signal occurred at 12 ppm, indicated that the protons at 2.0 ppm were associated with the

C atom adjacent to Fe. The protons at 2.10 ppm and 1.20 ppm were attached to the C appearing at 31 ppm, which illustrated that these two proton signals resulted from the CH_2 protons in the middle of the propyl spacer.

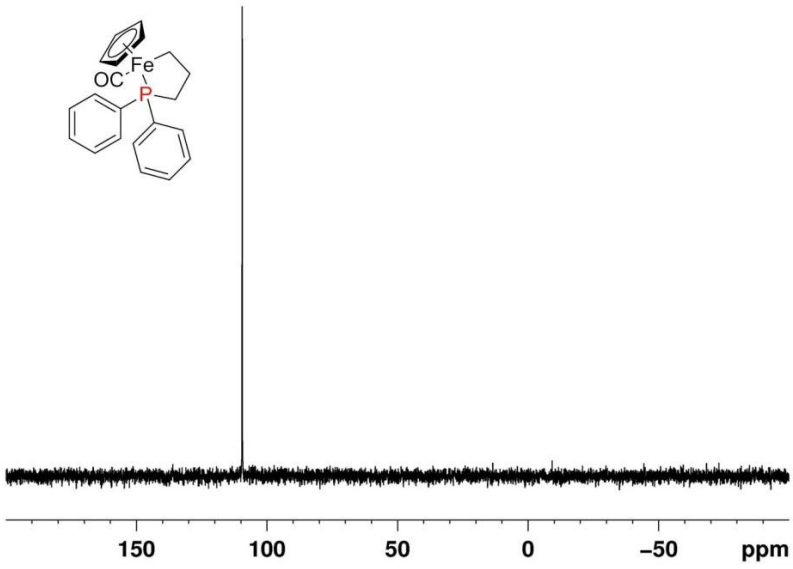

Figure 3.9 ^{31}P NMR spectrum of cyclic FpP5 in $CDCl_3$.

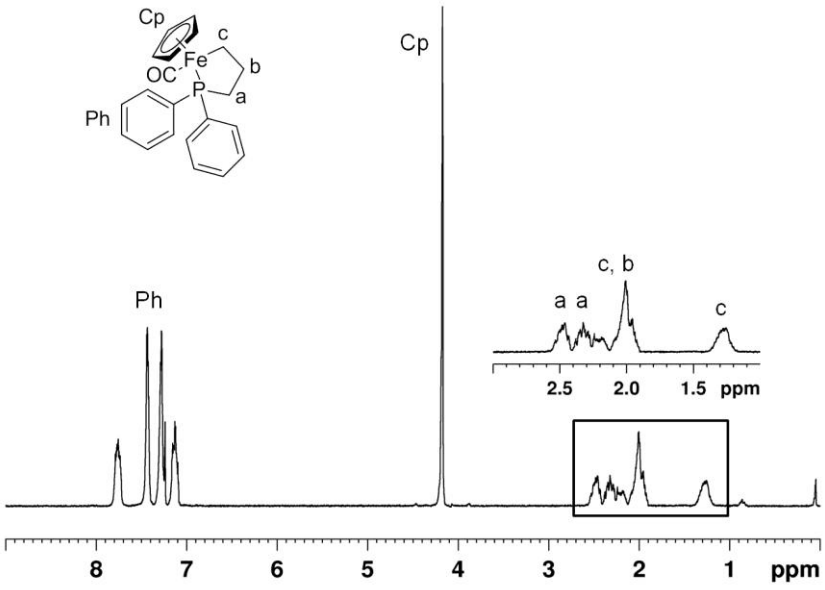

Figure 3.10 ^{1}H NMR spectrum of cyclic FpP5 in $CDCl_3$.

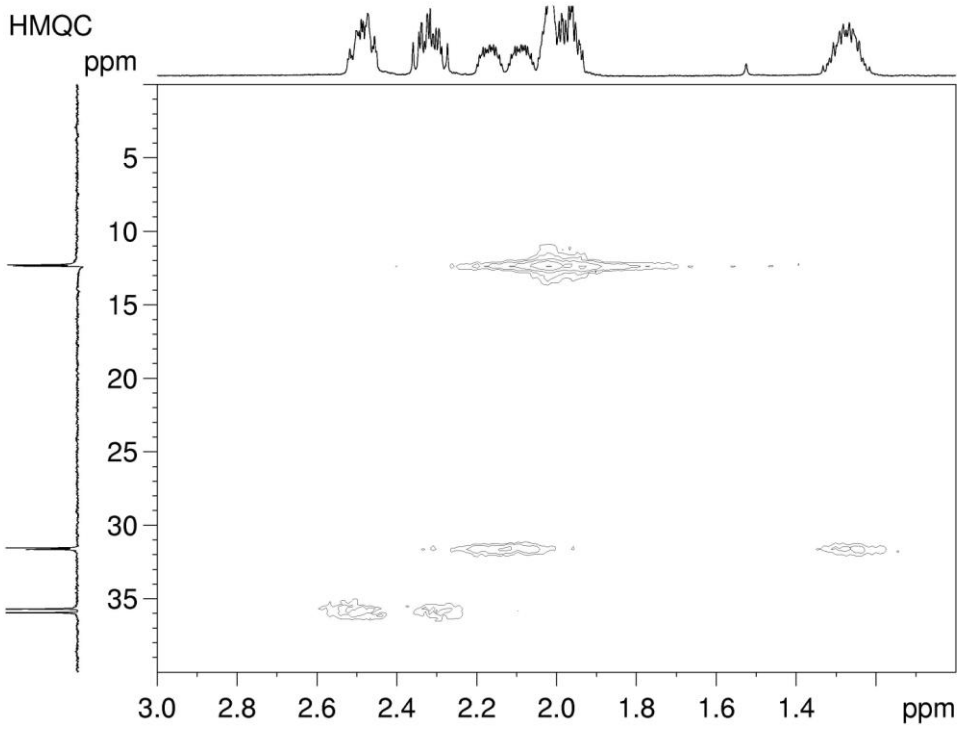

Figure 3.11 ^{1}H-^{13}C HMQC 2D NMR spectrum of cyclic FpP5 in $CDCl_3$.

3.3.2.2 Synthesis and characterization of cyclic FpP6

Cyclic FpP6 was produced by heating a dilute solution of FpP (10 mg/mL) at 70 ℃ in the dark. The cyclic FpP6 was confirmed from single-crystal XRD using a sample recrystallized at -49 ℃ from a hexane/DCM (5:1, v/v) solution. The compound crystallized in the monoclinic $P2_1/c$ space group. As shown in **Figure 3.12**, CO inserted into the Fe-C bond via MIR, thereby resulting in formation of a six-membered ring.

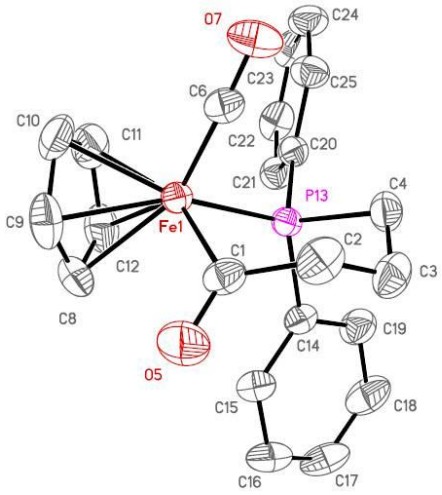

Figure 3.12 Crystal structure of cyclic FpP6 with thermal ellipsoids (50% probability level). Hydrogen atoms are omitted for clarity.

Cyclic FpP6 was characterized using ^{31}P NMR (**Figure 3.13**). The ^{31}P NMR spectrum shows a single peak at 70 ppm, which is consistent with phosphorus coordinated to the metal center via an MIR. The compound was also characterized using ^{1}H NMR (**Figure 3.14**), in which the Cp peak occurred at 4.5 ppm, while the signals at 7.5 ppm and 7.4 ppm were attributed to the phenyl group. As shown, three CH_2 groups in the propyl spacer showed signals at five different positions in the range of 2.8 ppm to 1.2 ppm. In order to assign these peaks, an ^{1}H-^{13}C HMQC 2D NMR experiment was performed (**Figure 3.15)**. The proton signals appearing at 2.80 ppm and 2.30 ppm were correlated to the C atom whose signal occurs at 60 ppm in ^{13}C NMR. This indicated that the peaks at 2.81 ppm and 2.30 ppm were due to the CH_2 group next to CO. The protons at 2.50 ppm and 2.30 ppm were associated with the C atom whose signal occurs at 29 ppm. This C showed a doublet signal, which is most likely due to the coupling of carbon with phosphorus.[69] This result illustrated that the signals at 2.50 ppm and

2.30 ppm arose from the CH_2 group next to phosphorus. The protons at 1.80 ppm and 1.30 ppm were attached to the C appearing at 20 ppm, indicating that these two signals resulted from the CH_2 protons in the middle of the propyl spacer. Although the ^{13}C signals were not observed in the ^{1}H-^{13}C HMQC 2D NMR spectrum, these peaks were observed in the ^{13}C DEPT-135 NMR spectrum of cyclic FpP6 (**Figure 3.16**).

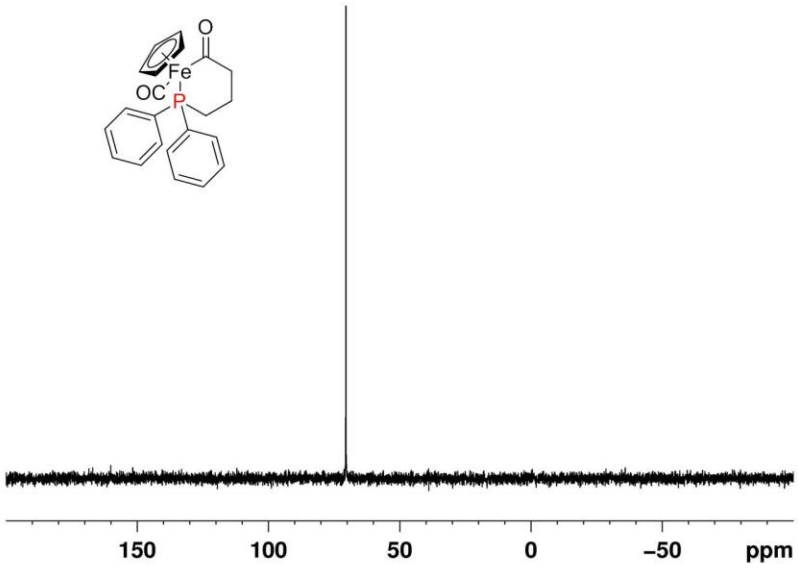

Figure 3.13 ^{31}P NMR spectrum of cyclic FpP6 in $CDCl_3$.

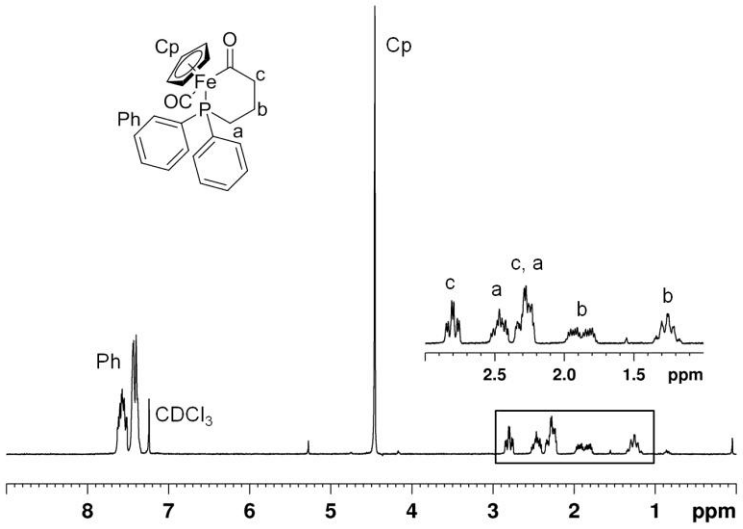

Figure 3.14 ^{1}H NMR spectrum of cyclic FpP6 in $CDCl_3$.

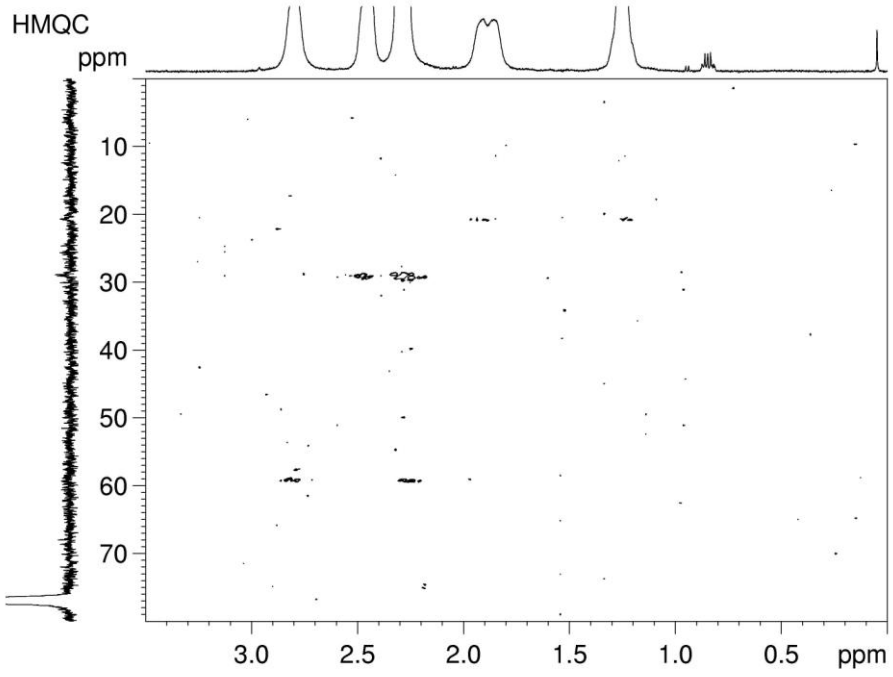

Figure 3.15 ^{1}H-^{13}C HMQC 2D NMR of cyclic FpP6 in $CDCl_3$.

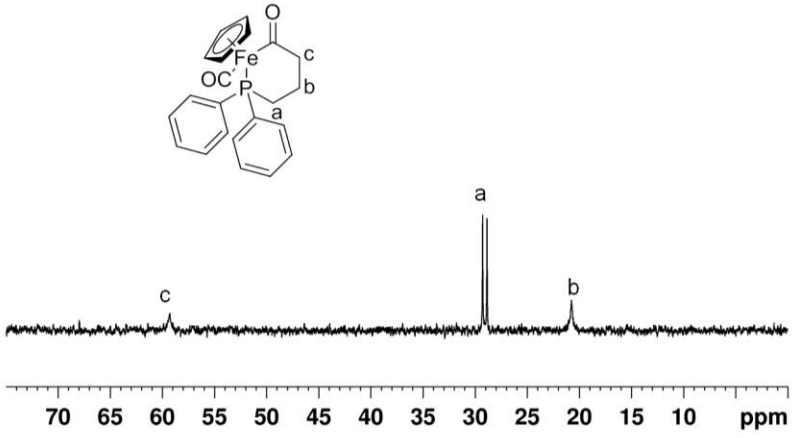

Figure 3.16 ^{13}C DEPT-135 NMR spectrum of cyclic FpP6 in $CDCl_3$.

3.4 Synthesis of PFpP

As MIR can occur in the solid state,[57] bulk polymerization of FpP was performed at 70-75 ℃ to suppress cyclization reactions. During polymerization, the viscosity of the system increased gradually, and the sample turned solid after ca. 1 h. The immobilized solid was continually heated for a designated time for further polymerization. The product is a glass-like transparent red-brown solid. To terminate the polymerization, the reactant was cooled to room temperature. The crude product was purified by dissolving in a minimal amount of THF (or DCM) followed by precipitation in hexane. A pale yellow precipitate was collected. After drying, a yellow powder was obtained which was readily soluble in THF, DMF, DCM, chloroform, benzene, DMSO and toluene.

3.4.1 PFpP structure characterization

In contrast to the FTIR spectrum of FpP, the FTIR spectrum of PFpP had two absorption frequencies, one at 1910 cm^{-1}, and the other at 1600 cm^{-1} (**Figure 3.17**). This indicated the presence of both terminal CO (C≡O) and inserted carbonyl groups (C=O).[56,70] This was further verified by ^{13}C NMR analysis (**Figure 3.18**) of the polymers, which showed resonance peaks at 219 ppm and 272 ppm, corresponding to terminal CO and acyl groups, respectively.[56]

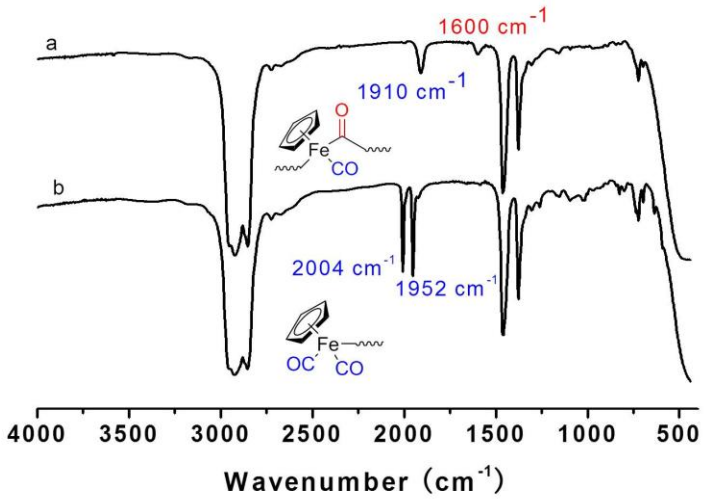

Figure 3.17 FTIR spectra of (a) PFpP and (b) FpP.

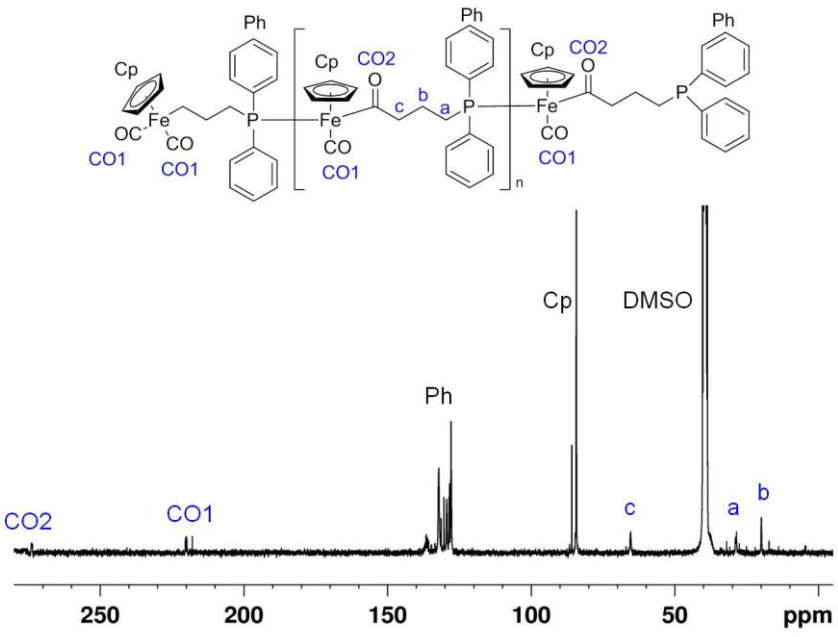

Figure 3.18 ^{13}C NMR spectrum of PFpP in DMSO-d_6.

PFpP obtained from bulk polymerization was also characterized using ^{31}P and ^{1}H NMR spectroscopies. In the ^{31}P NMR spectrum (**Figure 3.19**), three signals were observed: 73 ppm, 72 ppm and -13.7 ppm. These were attributed to the polymer repeat units,[54] the last repeat units of the polymer, and the uncoordinated polymer end group, respectively. In addition, the integrations of the signal at 72 ppm and -13.7 ppm were always equal, indicating they may be attributed to polymer chain ends. Taking advantage of the visible end-group signals, the degree of polymerization (DP) can be calculated from ^{31}P NMR.

The resulting polymer was also characterized by ^{1}H NMR spectroscopy in DMSO-d_6 (**Figure 3.20**). The peaks at 2.8 ppm and 2.3 ppm were assigned to the two diastereotopic protons from the $C(O)CH_2$ acyl groups, as they are adjacent to the Fe chiral center. The signal at 2.0-2.2 ppm was assigned to the protons adjacent to PPh_2, and 0.9-1.3 ppm was assigned to the central CH_2 protons. These signals had an integration ratio of 1:1. In addition, the Cp signal appeared at 4.3 ppm, which underwent a 0.5 ppm upfield shift compared to that of FpP (**Figure 3.4**), indicating that an MIR had occurred.[67] The signal at 7.8-7.1 ppm was attributed to the phenyl groups. The integration ratio of the Cp signal and phenyl protons signal was 1:2, corresponding to the numbers of protons in the expected structure. A small peak at 4.8 ppm was still observed, and was attributed to the end group of the polymer (**Figure 3.19**). The DP, therefore, could be calculated using the ratio of the peaks at 4.3 ppm and 4.8 ppm. It is noteworthy that the DPs calculated from ^{1}H NMR and ^{31}P NMR were highly consistent, as it was examined by several polymer samples.

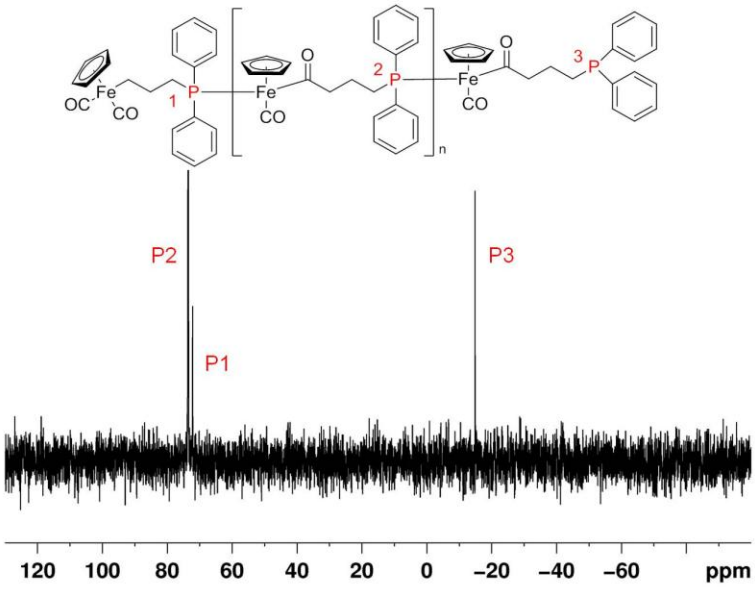

Figure 3.19 ^{31}P NMR spectrum of PFpP in DMSO-d_6 (integration ratio of P1:P2:P3 = 5:1:1).

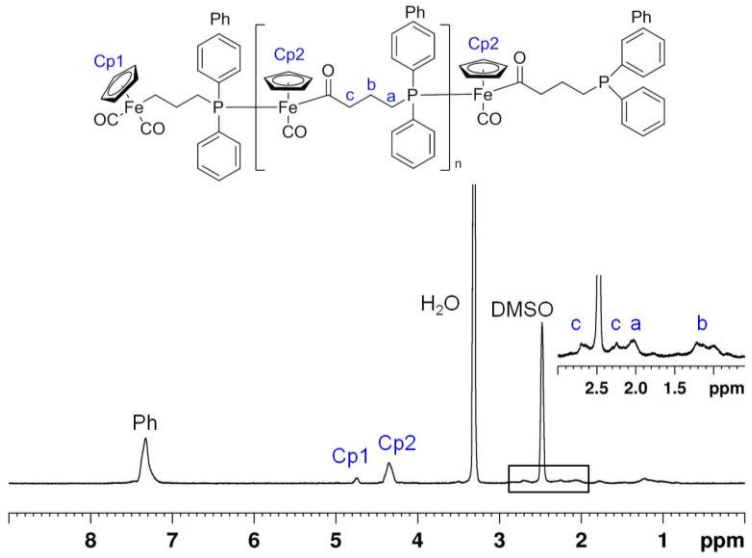

Figure 3.20 ^{1}H NMR spectrum of PFpP in DMSO-d_6 (integration ratio of Cp2:Cp1= 6:1).

PFpP was also characterized using UV-Vis spectroscopy (**Figure 3.21**). The measurement was carried out in THF with a PFpP concentration of 0.56 mmol/L. The compound showed a broad absorption between 330 nm and 500 nm.

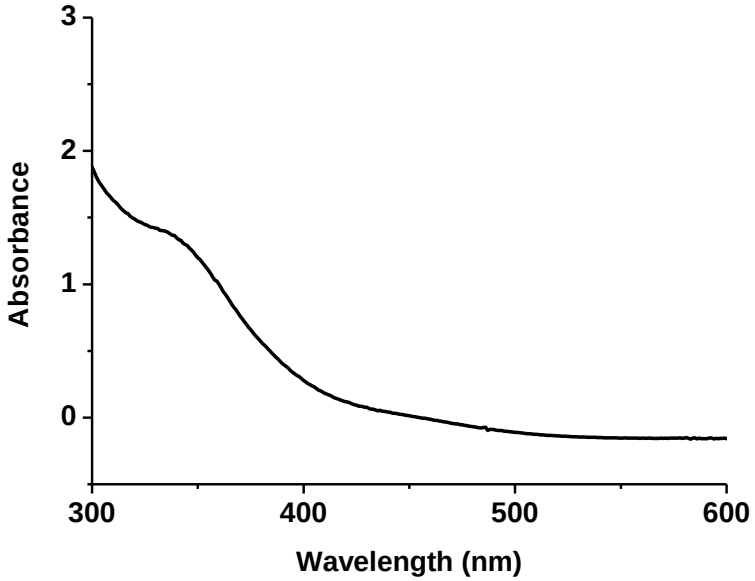

Figure 3.21 UV-Vis spectrum of PFpP (M_n = 3920 g/mol, PDI = 1.15) in THF (0.56 mmol/L).

3.4.2 PFpP molecular weight characterization

The macromolecular nature of the products was established by GPC analysis. The GPC results for the polymers are summarized in **Table 1**. The polymers were successfully synthesized with M_w up to 15500 g/mol and M_n up to 12100 g/mol. In addition, the DPs calculated from GPC and NMR are highly consistent, which indicates that the resulting molecules are linear polymer chains without

closed ring structure.

Table 1. GPC results for PFpP prepared from MIP of FpP

Time (h)	Temperature (℃)	M_w (g/mol)	M_n (g/mol)	PDI	DP	
					GPC	NMR
12	70	7240	6640	1.09	16	16
16	70	13090	9870	1.33	24	23
18	75	15500[1]	12100[1]	1.28[1]	30	-[2]

[1]Sample for GPC was taken right after the polymerization without purification

[2]End groups are invisible in NMR

3.4.3 Thermal properties of PFpP

Thermal properties of the polymers were studied by TGA and DSC. TGA (**Figure 3.21**) indicated that the polymer lost ca. 60 % of its original weight at 180 ℃. The second stage of weight loss started at 432 ℃, and the polymer lost ca. 77 % of its original weight at 622 ℃ leaving ca. 23% char yield. DSC analysis (**Figure 3.22**) indicated that the PFpP had a T_g at ca. 100 ℃, suggesting thermoplastic nature of the polymers.

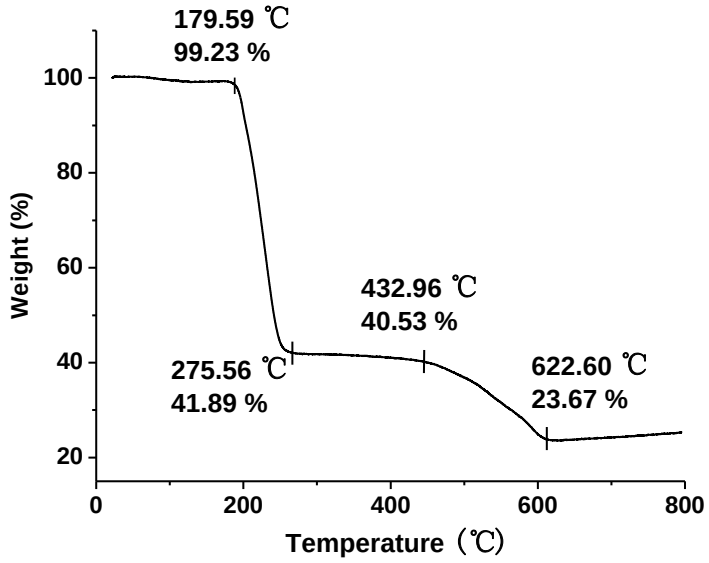

Figure 3.21 TGA of PFpP.

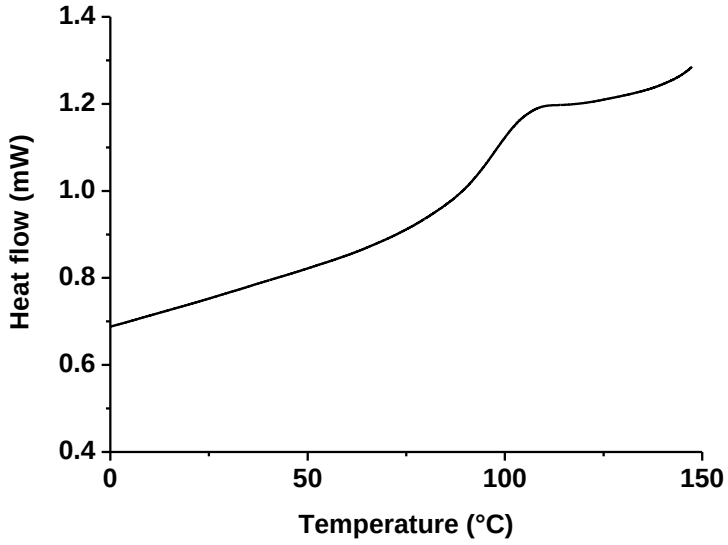

Figure 3.22 DSC analysis of PFpP.

Conclusions

MCPs have attracted increased attention in recent years because of their unique properties and functions. In comparison with the synthesis of side-chain MCPs, strategies for the synthesis of main-chain MCPs are limited. Therefore a new polymerization technique, MIP, was developed for the preparation of MCPs with Fe presented in the main chain. In this work, FpP was synthesized via the reaction between the Fp anion and $Ph_2PCH_2CH_2CH_2Cl$, and was characterized using FTIR, ^{1}H NMR, ^{31}P NMR, ^{13}C NMR, and UV-Vis spectroscopies. FpP readily underwent intramolecular cyclization reactions in diluted solution, producing cyclic FpP5 at room temperature (or at 70 ℃) in the light, or cyclic FpP6 at 70 ℃ in the dark. The structures of cyclic FpP5 and cyclic FpP6 were confirmed using single-crystal XRD, and the two compounds were characterized using ^{1}H NMR, ^{31}P NMR, and ^{1}H-^{13}C HMQC 2D NMR. MIP of FpP occurred in bulk at 70 ℃, leading to PFpP. The resulting PFpP was characterized using FTIR, ^{1}H NMR, ^{31}P NMR, ^{13}C NMR, and UV-Vis spectroscopies. The molecular weights of the polymers were characterized using GPC. It showed that polymers with M_n up to 12,000 g/mol and narrow PDIs were produced. PFpP contains Ph_2P-Fe and Fe-CO bonds in the polymer backbone, representing a new type of main-chain MCPs. The thermal analysis of PFpP revealed that the polymers were stable up to 180 ℃ and had a T_g at 100 ℃.

Future work

The successful synthesis of PFpP by MIP introduces a new technique for the synthesis of main-chain MCPs. The stability of these polymers offers opportunities for the next stage of investigation into its properties, including its redox properties because of the presence of Fe, or optical properties due to chiral centers in the polymer main chain. These properties can be characterized using cyclic voltammetry (CV) and circular dichroism (CD) spectroscopy, respectively. In addition, polymers with different chemical structures can be synthesized using this strategy via rational monomer design. For example, MIP of FpP with different carbon spacers is being studied in this group. Furthermore, PFpP chain ends produced via MIP are still reactive; using this property, various types of PFpP-containing block copolymers or PFpP-containing amphiphiles can be obtained. Subsequently, the self-assembly behaviors of these PFpP-based block copolymers or amphiphiles in solution are of interest for future research. For example, the micellization behaviors of $CH_3(CH_2)_9P(Ph)_2$-functionalized PFpP is being studied in this group. Finally, it has been reported that the photochemical treatment of FpR with phosphine ligands leads to decarbonylation of FpR with the phosphine coordinated to the empty site of Fe,[68] and the intramolecular cyclization reaction of FpP accompanied with decarbonylation was observed in this study. As a result, the photocontrolled polymerization of FpP may appear promising.

Permission

This thesis contains material that was reprinted (adapted) with permission from Wang, X.; Cao, K., Liu Y.; Tsang, B.; and Liew, S. *J. Am. Chem. Soc.* **2013**, *135*, 3399. Copyright (2013) American Chemical Society.

References

(1) Ho, C.-L.; Wong, W.-Y. *Coord. Chem. Rev.* **2011**, *255*, 2469.

(2) Whittell, G. R.; Manners, I. *Adv. Mater.* **2007**, *19*, 3439.

(3) Manners, I. *Synthetic Metal-Containing Polymers*; Wiley, 2004.

(4) Arimoto, F. S.; A. C. Haven, J. *J. Am. Chem. Soc.* **1955**, *77*, 6295.

(5) Schubert, U. S.; Eschbaumer, C. *Angew. Chem. Int. Ed.* **2002**, *41*, 2892.

(6) Williams, K. A.; Boydston, A. J.; Bielawski, C. W. *Chem. Soc. Rev.* **2007**, *36*, 729.

(7) Abd-El-Aziz, A. S.; Shipman, P. O.; Boden, B. N.; McNeil, W. S. *Prog. Polym. Sci.* **2010**, *35*, 714.

(8) Heilmann, J. B.; Scheibitz, M.; Qin, Y.; Sundararaman, A.; Jäkle, F.; Kretz, T.; Bolte, M.; Lerner, H.-W.; Holthausen, M. C.; Wagner, M. *Angew. Chem. Int. Ed.* **2006**, *45*, 920.

(9) Fukumoto, H.; Yamane, K.; Kase, Y.; Yamamoto, T. *Macromolecules* **2010**, *43*, 10366.

(10) Herbert, D. E.; Mayer, U. F. J.; Manners, I. *Angew. Chem. Int. Ed.* **2007**, *46*, 5060.

(11) Bellas, V.; Rehahn, M. *Angew. Chem. Int. Ed.* **2007**, *46*, 5082.

(12) Rulkens, R.; Ni, Y.; Manners, I. *J. Am. Chem. Soc.* **1994**, *116*, 12121.

(13) Qin, Y.; Cui, C.; Jäkle, F. *Macromolecules* **2008**, *41*, 2972.

(14) Ren, L.; Hardy, C. G.; Tang, C. *J. Am. Chem. Soc.* **2010**, *132*, 8874.

(15) Furuta, P. T.; Deng, L.; Garon, S.; Thompson, M. E.; Fréchet, J. M. J. *J. Am. Chem. Soc.* **2004**, *126*, 15388.

(16) Hanton, S. D. *Chem. Rev.* **2001**, *101*, 527.

(17) Whittell, G. R.; Hager, M. D.; Schubert, U. S.; Manners, I. *Nature Mater.* **2011**, *10*, 176.

(18) Dong, Q.; Li, G.; Ho, C.-L.; Faisal, M.; Leung, C.-W.; Pong, P. W.-T.; Liu, K.; Tang, B.-Z.; Manners, I.; Wong, W.-Y. *Angew. Chem. Int. Ed.* **2012**, *24*, 1034.

(19) Burnworth, M.; Tang, L.; Kumpfer, J. R.; Duncan, A. J.; Beyer, F. L.; Fiore, G. L.; Rowan, S. J.; Weder, C. *Nature* **2011**, *472*.

(20) Kishimura, A.; Yamashita, T.; Yamaguchi, K.; Aida, T. *Nature Mater.* **2005**, *4*, 546

(21) Nuyken, O.; Burkhardt, V.; Hiibsch, C. *Macromol. Chem. Phys.* **1997**, *198*, 3353.

(22) Baumert, M.; Fröhlich, J.; Stieger, M.; Frey, H.; Mülhaupt, R.; Plenio, H. *Macromol. Rapid Commun.* **1999**, *20*, 203.

(23) Higashihara, T.; Faust, R. *Macromolecules* **2007**, *40*, 7453.

(24) Tonhauser, C.; Mazurowski, M.; Rehahn, M.; Gallei, M.; Frey, H. *Macromolecules* **2012**, *45*, 3409.

(25) Gallei, M.; Schmidt, B. V. K. J.; Klein, R.; Rehahn, M. *Macromol. Rapid Commun.* **2009**, *30*, 1463.

(26) Herfurth, C.; Voll, D.; Buller, J.; Weiss, J.; Barner-Kowollik, C.; Laschewsky, A. *J. Polym. Sci., Part A: Polym. Chem.* **2012**, *50*, 108.

(27) Tonhauser, C.; Alkan, A.; Schömer, M.; Dingels, C.; Ritz, S.; Mailänder, V.; Frey, H.; Wurm, F. R. *Macromolecules* **2013**, *46*, 647.

(28) Ren, L.; Zhang, J.; Bai, X.; Hardy, C. G.; Shimizu, K. D.; Tang, C. *Chem. Sci.* **2012**, *3*, 580.

(29) Ren, L.; Hardy, C. G.; Tang, S.; Doxie, D. B.; Hamidi, N.; Tang, C. *Macromolecules* **2010**, *43*, 9304.

(30) Ren, L.; Zhang, J.; Hardy, C. G.; Ma, S.; Tang, C. *Macromol. Rapid Commun.* **2012**, *33*, 510.

(31) Zhang, J.; Ren, L.; Hardy, C. G.; Tang, C. *Macromolecules* **2012**, *45*, 6857.

(32) Chadha, P.; Ragogna, P. J. *Chem. Commun.* **2011**, *47*, 5301.

(33) AL-Badri, Z. M.; Maddikeri, R. R.; Zha, Y.; Thaker, H. D.; Dobriyal, P.; Shunmugam, R.; Russell, T. P.; Tew, G. N. *Nature Commun.* **2011**, *2*, 482.

(34) Zha, Y.; Thaker, H. D.; Maddikeri, R. R.; Gido, S. P.; Tuominen, M. T.; Tew, G. N. *J. Am. Chem. Soc.* **2012**, *134*, 14534.

(35) Chen, B.; Sleiman, H. F. *Macromolecules* **2004**, *37*, 5866.

(36) Chen, B.; Metera, K.; Sleiman, H. F. *Macromolecules* **2005**, *38*, 1084.

(37) Sankaran, N. B.; Rys, A. Z.; Nassif, R.; Nayak, M. K.; Metera, K.; Chen, B.; Bazzi, H. S.; Sleiman, H. F. *Macromolecules* **2010**, *43*, 5530.

(38) Hou, S.; Man, K. Y. K.; Chan, W. K. *Langmuir* **2003**, *19*, 2485.

(39) Bignozzi, C. A.; Ferri, V.; Scoponi, M. *Macromol. Chem. Phys.* **2003**, *204*, 1851.

(40) Roy, X.; Hui, J. K.-H.; Rabnawaz, M.; Liu, G.; MacLachlan, M. J. *Angew. Chem. Int. Ed.* **2011**, *50*, 1597.

(41) Roy, X.; Hui, J. K.-H.; Rabnawaz, M.; Liu, G.; MacLachlan, M. J. *J. Am. Chem. Soc.* **2011**, *133*, 8420.

(42) Liu, Y.; Wang, X. *Polym. Chem.* **2012**, *3*, 2632.

(43) Wang, S.; Li, X.; Xun, S.; Wan, X.; Wang, Z. Y. *Macromolecules* **2006**, *39*, 7502.

(44) Lin, W.; Zheng, Y.; Zhang, J.; Wan, X. *Macromolecules* **2011**, *44*, 5146.

(45) Nguyen, P.; Gómez-Elipe, P.; Manners, I. *Chem. Rev.* **1999**, *99*, 1515.

(46) Foucher, D. A.; Tang, B. Z.; Manners, I. *J. Am. Chem. Soc.* **1992**, *114*, 6246.

(47) Rulkens, R.; Lough, A. J.; Manners, I. *J. Am. Chem. Soc.* **1994**, *116*, 797.

(48) Gädt, T.; Ieong, N. S.; Cambridge, G.; Winnik, M. A.; Manners, I. *Nature Mater.* **2009**, *8*, 144.

(49) Rupar, P. A.; Chabanne, L.; Winnik, M. A.; Manners, I. *Science* **2012**, *337*, 559.

(50) Tanabe, M.; Manners, I. *J. Am. Chem. Soc.* **2004**, *126*, 11434.

(51) Gilroy, J. B.; Patra, S. K.; Mitchels, J. M.; Winnik, M. A.; Manners, I. *Angew. Chem. Int. Ed.* **2011**, *50*, 5851.

(52) Wang, X.; Guerin, G.; Wang, H.; Wang, Y.; Manners, I.; Winnik, M. A. *Science* **2007**, *317*, 644.

(53) Yusoff, S. F. M.; Hsiao, M.-S.; Schacher, F. H.; Winnik, M. A.; Manners, I. *Macromolecules* **2012**, *45*, 3883.

(54) Sharma, H. K.; Cervantes-Lee, F.; Pannell, K. H. *J. Am. Chem. Soc.* **2004**, *126*, 1326.

(55) Harting, J. F. *Organotransition Metal Chemistry From Bonding to Catalysis*; University Science Books: Sausalito, California, 2010.

(56) Kumar, M.; Metta-Magana, A. J.; Sharma, H. K.; Pannell, K. H. *Dalton Trans.* **2010**, *39*, 7125.

(57) Theysa, R. D.; Dudleyb, M. E.; Hossainb, M. M. *Coord. Chem. Rev.* **2009**, *253*, 180.

(58) APEX2, User Manual; Bruker AXS Inc.: Madison, WI, 2006.

(59) Aladzheva, I. M.; Bykhovskaya, O. V.; Lobanov, D. I.; Petrovskii, P. V.; K. A. Lysenko; Mastryukova, T. A. *Chem. Heterocycl. Compd.* **2002**, *38*, 95.

(60) Uriarte, R.; Mazanec, T. J.; Tau, K. D.; Meek, D. W. *Inorg. Chem.* **1980**, *19*, 79.

(61) Gladysz, J. A.; Williams, G. M.; Tam, W.; Johnson, D. L.; Parker, D. W.; Selover, J. C. *Inorg. Chem.* **1979**, *18*, 553.

(62) Regera, D. L.; Fautha, D. J.; Dukesa, M. D. *Synth. React. Inorg. Met.-Org. Chem.* **1977**, *7*, 151.

(63) Mapolie, S. F.; Moss, J. R.; Smith, G. S. *Appl. Organomet. Chem.* **1998**, *12*, 801.

(64) Plotkin, J. S.; Shore, S. G. *Inorg. Chem.* **1981**, *20*, 284.

(65) Moss, J. R. *J. Organomet. Chem.* **1982**, *231*, 229.

(66) Hermans, L.; Mapolie, S. F. *Polyhedron* **1997**, *16*, 869.

(67) Scharrer, E.; Brookhart, M. *J. Organomet. Chem.* **1995**, *497*, 61.

(68) Pannell, K. H.; Sharma, H. K. *Organometallics* **2010**, *29*, 4741.

(69) Ferna ́ndez, I.; lez, J. G.; pez-Ortiz, F. L. *J. Am. Chem. Soc.* **2004**, *126*, 12551.

(70) Luh, L.-S.; Liu, L.-K. *Organometallics* **1995**, *14*, 1514.

(71) Grim, S. O.; Barth, R. C. *J. Organomet. Chem.* **1975**, *94*, 327.

Appendix

A1. Kinetic study of MIP

A kinetic study was carried out in order to explore the polymerization mechanism of MIP. This kinetic study was carried out at 70 ℃ in bulk. Samples were collected at specific times. Each sample was dissolved in $CDCl_3$, without any purification for ^{31}P NMR and ^{1}H NMR analysis.

Typical ^{31}P and ^{1}H NMR spectra are shown in **Figure A1** and **Figure A2** (a sample collected at 5 h was used as an example). The signals in each spectrum could be assigned clearly. As can be seen from the ^{31}P NMR spectrum (**Figure A1**), every peak that appeared in the spectra were assigned as follows: 109 ppm (cyclic FpP5), 73 ppm and 72 ppm (P-Fe linkages in the middle of polymer chain upon migration and P-Fe linkage at the polymer chain end upon migration), 69 ppm (cyclic FpP6), -13.6 ppm (polymer chain end) and -14.2 ppm (unreacted monomer).

Cp ring peak assignment in a typical ^{1}H NMR spectrum is shown in **Figure A2**. The peaks were assigned as follows: 4.67 ppm (unreacted monomer), 4.56 ppm (polymer chain end), 4.47 ppm (cyclic FpP6), 4.33 ppm (polymer chain) and 4.18 ppm (cyclic FpP5). In addition, the Cp ring signal in the ^{1}H NMR spectrum for the purified polymer (heated for 5 h) is shown in **Figure A3**. Following purification, only two peaks, at 4.56 ppm and 4.33 ppm, appeared on the spectrum. This result further confirmed that the peaks at 4.56 ppm and 4.33 ppm resulted from the polymer. Furthermore, the integration ratio of these two peaks was 1: 3.19, which was consistent with that of unpurified polymer.

This result illustrated that the 4.56 ppm was attributed to the chain end and the 4.33 ppm was attributed to the polymer.

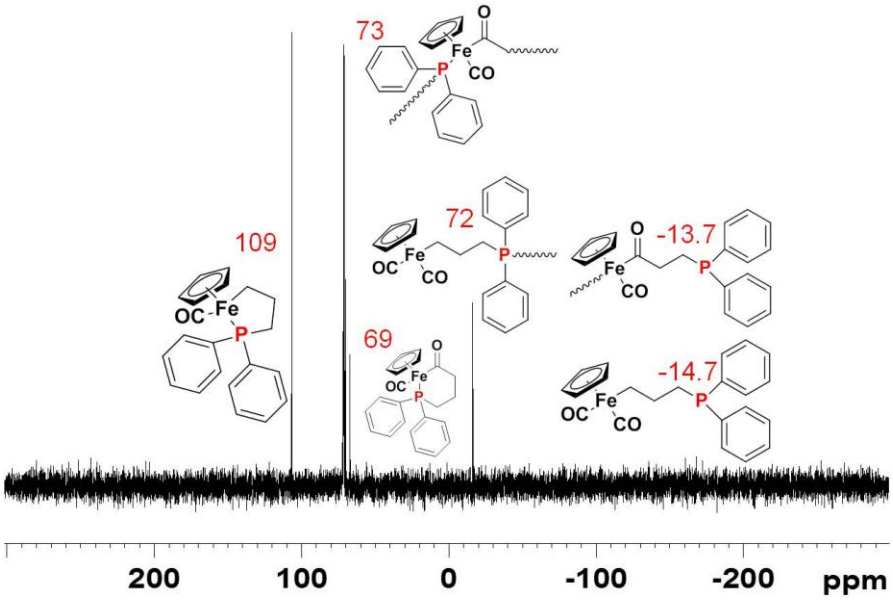

Figure A1 Typical ^{31}P NMR spectrum obtained in the kinetic study (sample prepared by directly dissolving the crude product in $CDCl_3$ without any purification; sample was heated for 5 h).

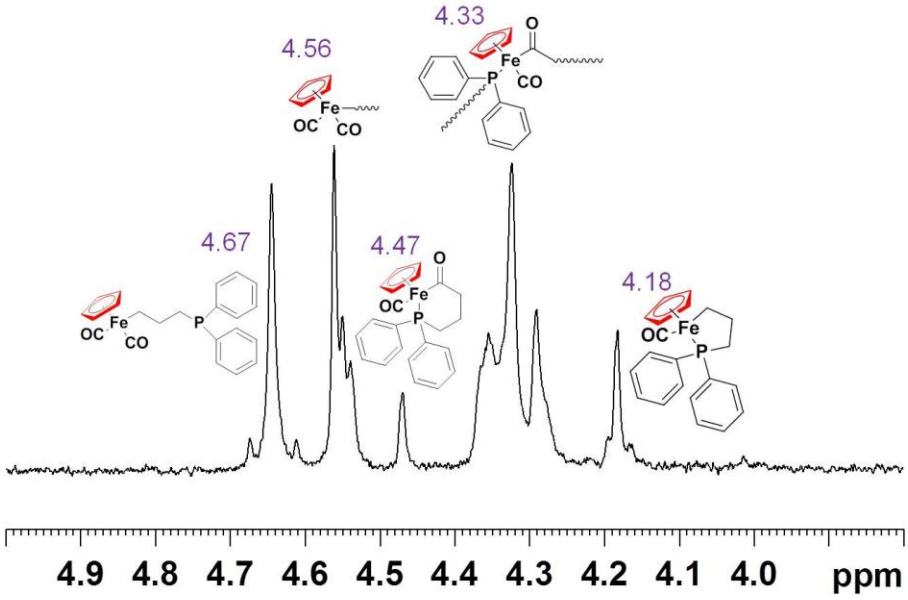

Figure A2 Typical ^{1}H NMR spectrum obtained in the kinetic study (sample prepared by directly dissolving the crude product in $CDCl_3$ without any purification; sample was heated for 5 h).

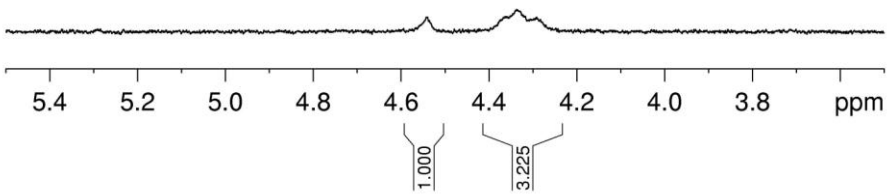

Figure A3 ^{1}H NMR of purified kinetic sample (sample was prepared by dissolving the purified polymer in $CDCl_3$; sample was heated for 5 h).

By taking advantage of the clear assignments for each peak in the ^{31}P NMR and ^{1}H NMR spectra, the monomer conversion and DP of each sample could be calculated. The monomer conversions and DPs calculated from ^{31}P NMR and ^{1}H NMR are shown in **Table A1**.

Table A1 The table of conversions and DPs calculated from ^{31}P NMR and ^{1}H NMR spectra

Sample	Time (h)	^{31}P		^{1}H	
		Conv. (%)	DP	Conv. (%)	DP
1	0.167	28.07	2.04	29.33	2.30
2	0.333	51.64	2.51	51.20	2.38
3	0.5	67.29	2.45	66.30	2.58
4	0.667	75.17	2.84	75.59	2.75
5	0.833	82.67	2.96	82.55	2.86
6	1	81.00	2.97	81.09	2.90
8	3	79.48	3.39	81.82	3.23
9	4	89.59	4.30	88.50	3.54
10	5	97.70	4.20	97.88	3.94
11	15.5	~ 100	7.69	~ 100	6.18

As seen in **Table A1**, the conversions and DPs calculated from ^{31}P NMR and ^{1}H NMR are highly consistent. The plots of the conversion vs. DP are shown in **Figure A4**, both plots show that polymerization followed the condensation polymerization trend.

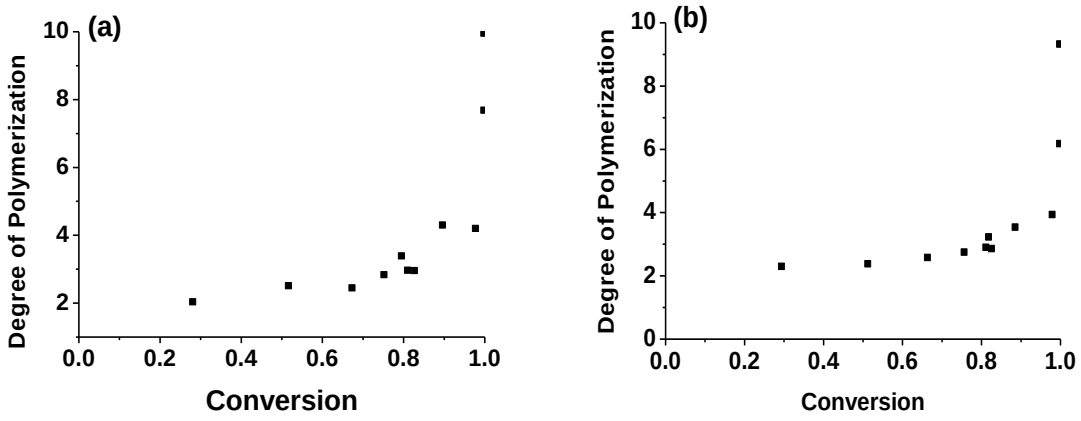

Figure A4 Plot of DP vs. conversion: (a) based upon ^{31}P NMR and (b) based upon ^{1}H NMR.

A2. PFpP stability in solution

The stability of PFpP in solution was also tested. The polymer solution (~ 0.005 mg/mL) was dissolved in six different solvents, including benzene, chloroform, DCM, DMF, THF, and toluene. These polymer solutions were stored under an atmosphere of N_2 at room temperature for 10 days, after which samples were collected for ^{31}P NMR analysis.

All the polymer solutions were originally clear yellow solutions. After 10 days, all the solutions had turned orange, and no precipitate was observed except for the sample in chloroform, which had turned brown, and a brown precipitate was observed. The samples in benzene, DCM, DMF, THF and toluene showed similar ^{31}P NMR after 10 days. For example, the ^{31}P NMR of THF solution is shown in **Figure A5**. The signal around 70 ppm became multiple. Meanwhile, a signal appeared at 109 ppm.

For the sample in chloroform (**Figure A6**), only the signal at 109 ppm was detected in solution, as the polymer has likely precipitated. These results indicated that the polymer changed when incubated in solution for long periods of time, particularly in $CDCl_3$, in which decomposition was observed.

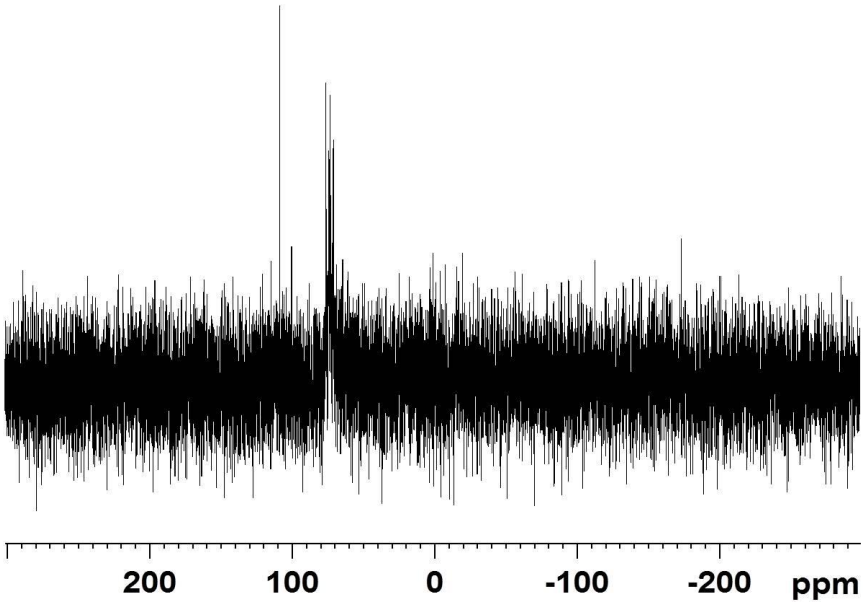

Figure A5 ^{31}P NMR spectrum of polymer in THF after 10 days.

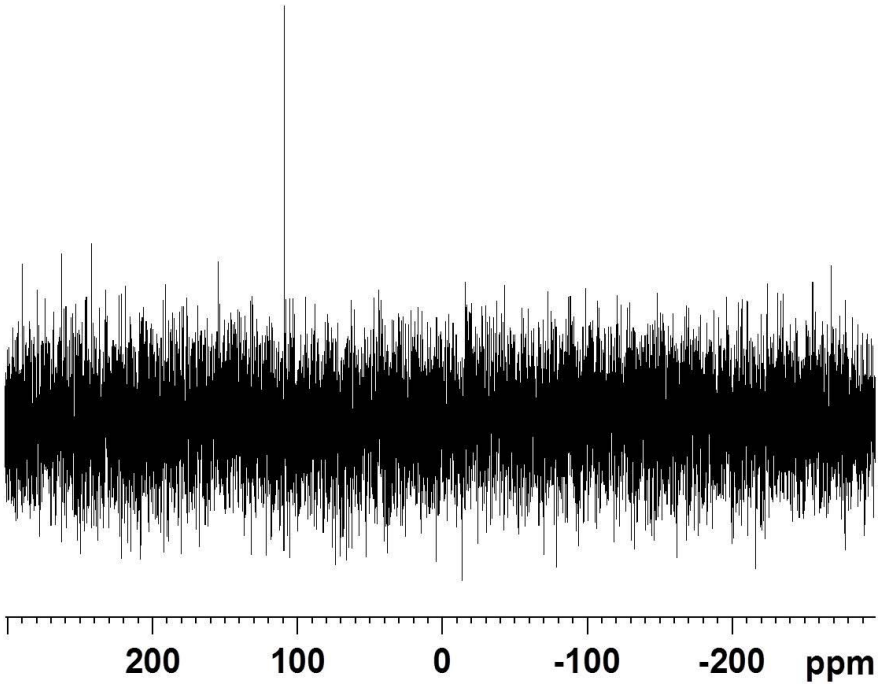

Figure A6 ^{31}P NMR spectrum of polymer in $CDCl_3$ after 10 days.

A3. Polymerization of FpP at 110 ℃

Polymerization was also carried out at 110 ℃ for 48 h in bulk. During the heating, the reactant was solidified, but remained soft. During the first 24 h, the reactant was initially a red-brown soft solid, but became a dark brown oil on the second day. After heating for 48 h, the sample showed low solubility in THF, likely caused by thermal decomposition.

A4. Synthesis of $Ph_2PCH_2CH_2Br$

Alkylation of Ph_2PNa with 1,2-dibromopropane in THF was attempted to prepare $Ph_2PCH_2CH_2Br$.

Following the reaction, the crude product was directly taken for ^{31}P NMR analysis. Only a single peak in the ^{31}P NMR spectrum was observed at -14.1 ppm, thus suggesting that the designed compound was obtained. However, upon evaporation of the solvent, multiple signals ranging from 31 ppm to 22 ppm were observed in the ^{31}P NMR spectrum, thereby indicating that the compound had decomposed upon solvent evaporation. It has been reported in the literature that the haloalkyl diphenylphosphine with short alkyl spacer is not stable and cannot be isolated.[71]

A5. NMR characterization of the product synthesized by using K[HBEt$_3$] reduced FpK and Ph$_2$PCH$_2$CH$_2$CH$_2$Cl.

After chromatography purification, the band eluted using EA was collected as a brown powder. ^{31}P NMR ($CDCl_3$): 54 ppm (**Figure A7**). ^{1}H NMR ($CDCl_3$): 7.9-7.0 ppm (broad peak), 5.1-4.6 ppm (broad peak), and 3.0-0.8 ppm (broad peak) (**Figure A8**).

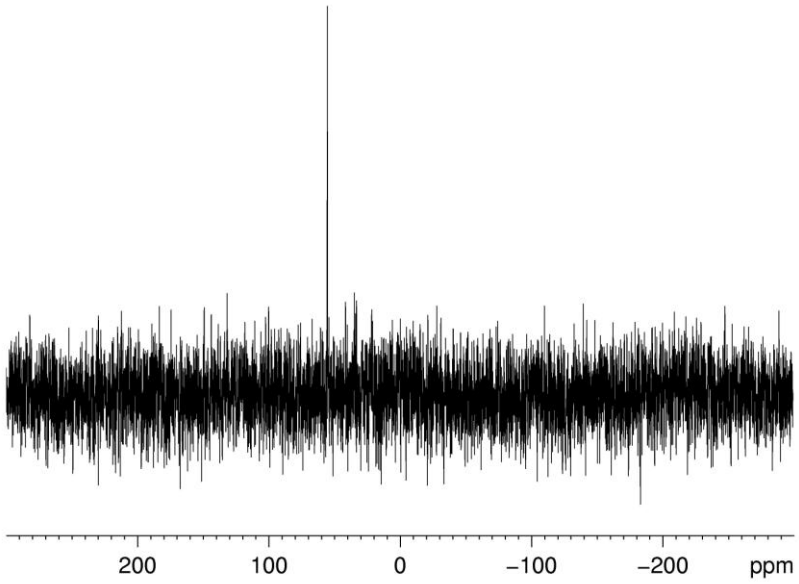

Figure A7 ^{31}P NMR spectrum of the unknown brown powder in $CDCl_3$.

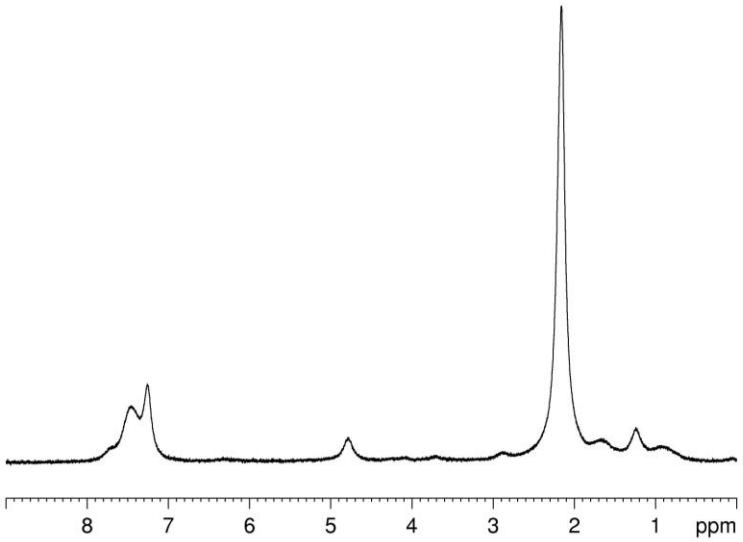

Figure A8 ^{1}H NMR spectrum of the unknown brown powder in $CDCl_3$.

A6. Alternative route for the synthesis of FpP

One of my colleagues attempted to synthesize FpP following **Scheme A1**, but resulting in cyclic FpP6 as the major product once. In order to investigate the effect of Ph_2PNa concentration on this reaction, reactions with different $Cp(CO)_2Fe(CH_2)_3Cl$ to Ph_2PNa ratios (1:1, 1:5 and 1:10), were performed. However, in cases with lesser amounts of $NaPPh_2$ (1:1 and 1:5), only FpP was produced as desired in **Scheme A1**. With larger amounts of Ph_2PNa (1: 10), less than 20 % cyclic FpP6 was obtained.

Scheme A1 Alternative route for the synthesis of FpP.